Bulging 9 weeks
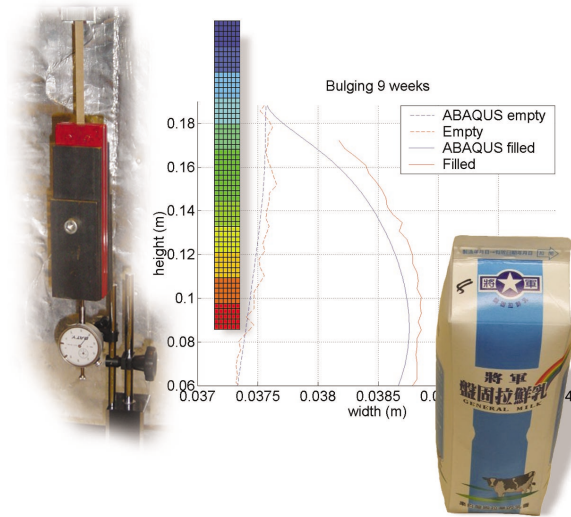
ANALYSIS OF CREEP IN PAPERBOARD PACKAGES WITH PLASTIC TOPS

JAKOB ARVIDSSON and JESPER GRÖNVALL

Master's Dissertation

Structural Mechanics

ANALYSIS OF CREEP IN PAPERBOARD PACKAGES WITH PLASTIC TOPS

Master's Dissertation by

Jakob Arvidsson och Jesper Grönvall

Supervisors:

Kent Persson, Div. of Structural Mechanics

Eskil Andreasson, Tetra Pak R&D AB

ACKNOWLEDGEMENT

Abstract

Beverage packages made of paper and plastic materials that are stored for a long time, deform due to creep deformations. The phenomena is termed bulging and means that the package changes its shape. Bulging is a major issue for the producers of beverage packages.

The purpose of this master's dissertation, is to develop a Finite Element-model for simulation of bulging of beverage packages at varying loadings and time scales that is verified to experimentally determined data of creep.

In order to formulate a suitable FE-model for simulation of creep, a profound knowledge of the material behavior of the various materials in a beverage package is required. Therefore, creep tests of paper, polymer, and aluminum foil were performed. The creep deformation of paper was found to be approximately four to six times larger in CD than in MD. The elastic + creep deformation of the laminate is approximately three times larger in CD in comparison to MD.

A creep material model for each of the materials in the laminate was calibrated to experimental data. The creep behavior of the FE-model was compared to bulge tests, which described the deflection of the package. The FE-model was proven to produce accurate results for shorter time periods and acceptable results for longer time frames.

As experimental creep tests require long time frames, it is important to anticipate the creep behavior with a mathematical model. The FE-method was shown to be an excellent tool in order to describe, understand, and predict the phenomena of creep.

Keywords: creep, beverage package, paper properties, FEM, ABAQUS, Power-law, crease.

Dictionary

anisotropy   different material properties in different directions.

compliance   a measure of a materials willingness to deform [4].

creep   time-dependent slowly increased deformation
by material exposed to a mechanical load [21].

dissipation   transformation of mechanical energy into heat [5].

orthotropy   a material possess two or three symmetrical planes.

relaxation   the applied stress on a specimen attached to a
device, decreases as a function of the time, i.e.
the strain is kept constant and the stress
decreases over time [21].

residual stress   stress that remains in a material after the manufacturing.

rheology   the study of deformation and flow of materials [4].

tensors   are quantities that change in a particular manner
when the coordinate system is changed [22].

viscosity   describing the flow-property of fluids, i.e. liquids
and gases, due to the inner friction of the fluid [21].

viscoelasticity   a combination of elastic and viscous properties
of a material [21].

Contents

1. Introduction

1.1. Background

Packages made from paper and plastics have many advantages compared to packages made from other materials, e.g. paper and plastics are easy to manufacture and are environment-friendly. A drawback is that beverage packages made of paper and plastic materials stored for a long time, deform due to creep deformations, causing swelling of the packages, which adopt the shape of a "balloon", shown in Figure 1.1. This phenomena is called bulging. In the end the final customers, i.e. you and I, will think that the content is fermented and will pick another package. Thus, the swelled packages will be rejected and unsold.

As experimental creep tests require long time frames, it is important to be able to anticipate the creep behavior with a mathematical model. The FE-method is an excellent tool in order to describe, understand, and predict the phenomena of creep.

Figure 1.1: *Bulging of a beverage package.*

1.2. Objectives

The main objectives in this master's dissertation are to investigate whether any of the available creep models in the computer program ABAQUS are suitable for describing bulging of a beverage package and to find experimental data to such a model. The work in this thesis is divided into four subtasks:

- Literature study of creep in paper and plastics

- Perform a survey of available creep models in ABAQUS

- Experimental study of creep with various materials, loading and time scales

- Development and verification of a FE-model for simulation of creep in beverage packages

The conclusive aim is to establish a material model, which would be applicable on various Tetra Pak packages.

2. Beverage Packages

2.1. General Remarks

In this chapter some basic information about beverage packages are discussed. More information about the subject is given in [1].

Paper packages are usually filled with fluids, e.g. milk or water, but they may also be filled with particles, i.e. food. The main part of the packages usually consists of paper material, but also contains various types of other materials. The top of the package, for example, sometimes consist of plastic material, e.g. Tetra Top. Tetra Pak manufactures many different types of packages, the most common are presented in Figure 2.1.

Within Tetra Pak, several abbreviations are used for packages. TBA is one of these abbreviations, where the first letter T stands for Tetra. The second letter B, which stands for Brick, defines the shaped geometry of the package. In this case, B says the package is rectangular shaped. Other designations of the shaped geometry are P-Prisma and W-Wedge. The last letter, A, indicates the package is aseptic, which means the filling and sealing process make the content free from bacteria. Consequently, the product does not need to be refrigerated. Thus, TBA is an abbreviation for Tetra Brick Aseptic. Other names used are Tetra Base, Tetra Slim, and Tetra Square.

Figure 2.1: *Tetra Pak packages, from left to right: Tetra Classic, Tetra Wedge, Tetra Rex, Tetra Prisma, Tetra Brik, Tetra Fino, Tetra Top, PET bottles and EBM bottles [1].*

Packages with different properties are made to satisfy several types of customers. For instance, TPA is developed as a more exclusive beverage package, unlike the low cost version TFA, which is developed for the emerging markets. TWA packages are usually made for small-portions of fluids and TBA is the most common ordinary package.

2.2. Materials in Packages

The material in a beverage package is a laminate that is organized in different layers. Typically, the laminate consist of paper, polyethylene, and aluminium foil. Each layer has specific properties. Paper consist of wood fibers, where the orientation depends on the manufacturing process. Fibers have a tendency to be oriented in the Machine Direction, shortened MD. The directions are illustrated in Figure 2.2, where CD is the cross-machine direction and the Z-direction denotes the direction out of the MD-CD plane. These are frequently used as the principal directions of paper. In almost every beverage package made by Tetra Pak, MD is oriented in the vertical height direction.

The material composition of the laminate layers in the packaging material, are different for each package. For instance, the layers in a package (from the inside to the outside) may be: three layers of LDPE (Low Density Polyethylene), aluminium foil, LDPE, paper, and finally an exterior surface of LDPE as shown in Figure 2.3.
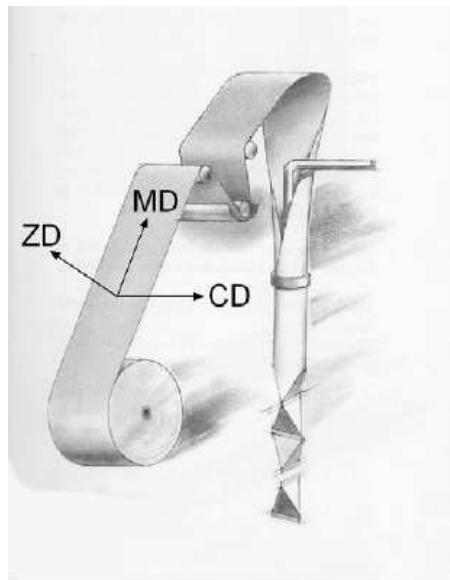
Figure 2.2: *The directions defining Machine Direction (MD), Cross machine Direction (CD) and Z-Direction (ZD) [1].*

Outside

LDPE

Paper

LDPE

Aluminium foil

Film LLDPE / LDPE

Inside
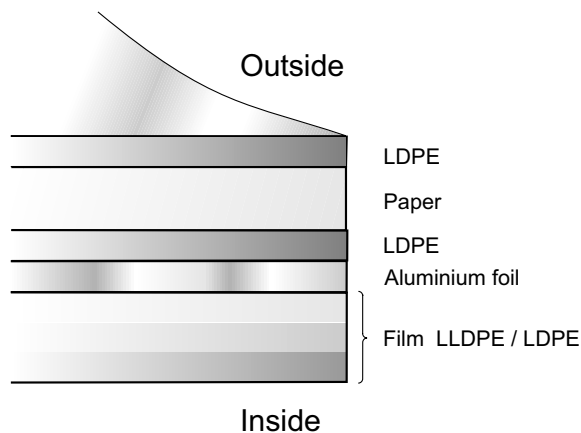
Figure 2.3: *The layers of a laminate.*

Since paper is the major material component of the package, the bulging is highly dependent on the properties of the paper. To get a non-diffusive package and to protect the content from light, a thin aluminium foil is used. The printing on the package is protected by the outer polyethylene layer. This layer and the inner polyethylene layers protect the paper from moisture. The intermediate polyethylene layer is gluing the aluminium foil and the paper together.

During the manufacturing of the package, the paper is creased to simplify the folding of the laminate. A crease is made by pressing a channel into the paper or board as the result of a scoring or grooving operation [2]. The appearance of a crease is displayed in Figure 2.4.
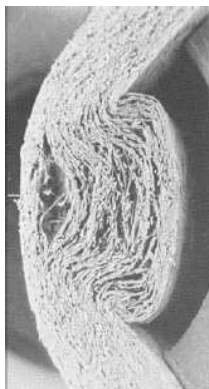
Figure 2.4: *Micrograph of the cross-section of a crease [1].*

2.3. Manufacturing of Packages

The process of manufacturing packages basically consists of six steps; printing, creasing, lamination, forming, filling, and finally sealing. The first step, printing, gives the paper material its final appearance. In the third step, the aluminium foil is laminated together with the paper, glued by melted polyethylene. The complete material is produced by applying the remaining two polyethylene layers. The folding, filling and sealing process are made in the filling machine to complete the manufacturing of a beverage package. The principle of the filling and sealing process of a package type TBA is shown in Figure 2.5.
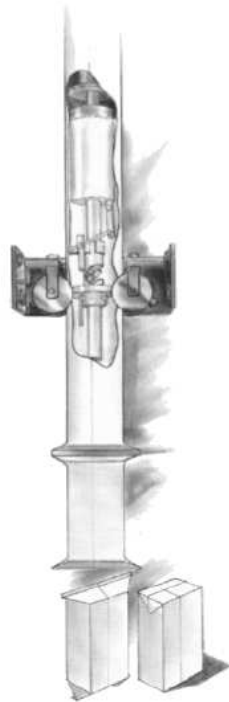
Figure 2.5: *The principal of the filling and sealing process of package type TBA [1].*

3. CONSTITUTIVE MODELS

3.1. General Remarks

This chapter presents a survey of the models describing the physical behavior of the materials in the beverage packages. The time-dependent long-term properties of paper and polymer may be modelled in several ways. In this chapter, a number of constitutive models are investigated. An overview of the creep models available in the general purpose FE-program ABAQUS, is also presented.

3.2. Linear Elastic Behavior

At pure elastic deformation the emerged stress depends merely on the imposed strain. The storage of the strain energy supplied to the material, is recovered when the material is relieved, i.e. the elastic deformation is reversible.

As long as the elastic deformation is sufficiently small, a linear constitutive description is suitable. In a cartesian coordinate system (x_1, x_2, x_3), the linear constitutive equation for a infintesimal strain ϵ_{kl} can be formulated according to

$$\sigma_{ij} = D_{ijkl}\epsilon_{kl} \tag{3.1}$$

where summation convention is used and the elastic tensor D_{ijkl} is a symmetrical fourth order tensor [3]. The so-called summation convention in index notation claims that if an index is repeated twice, then summation over this index is performed. The corresponding equation in matrix notation, is convenient for calculations and takes the following form

$$\boldsymbol{\sigma} = \boldsymbol{D} \cdot \boldsymbol{\epsilon} \tag{3.2}$$

where $\mathbf{D}$, is the flexibility matrix describing the elasticity and is for elastic materials a symmetrical matrix. For an anisotropic material (non-symmetric material), the dimension of $\mathbf{D}$ is 6×6 with 21 independent material constants.
In order to obtain an expression suitable to interpret the experimental data, simply invert the Eq. (3.2) and the inversion yields

$$\boldsymbol{\epsilon} = \boldsymbol{C} \cdot \boldsymbol{\sigma} \tag{3.3}$$

where $\boldsymbol{C} = \boldsymbol{D}^{-1}$ denotes the stiffness matrix [19].

Ordinary materials, usually consists of a couple of internal symmetries. Therefore, a number of irrespective components is reduced in the elastic matrix. For a linear isotropic pure elastic material, the general constitutive equation Eq. (3.1), may be written as

$$\sigma_{ij} = \left(K - \tfrac{2}{3}G \right) \epsilon_{kk}\delta_{ij} + 2G\epsilon_{ij} \tag{3.4}$$

where δ_{ij} is Kroneckers delta [3]. The bulk modulus (K) describes the volumetric change of the material exposed to a hydrostatic pressure. Further, the shear modulus (G) corresponds to the change of shape. At uniaxial tensile load in the x_1-direction, the following relation between stress and strain is obtained

$$\sigma_{11} = E\epsilon_{11} \tag{3.5}$$

where E denotes the modulus of elasticity [3].

3.3. Creep

Creep can be defined as a progressive increase of strain in a material exposed to a constant load, observed over an extended period of time. The three types of dynamic tests are creep, recovery, and stress relaxation. Creep tests involve a sample with a set weight and observation of the strain change over time. Recovery tests look at how the material relaxes once the load is removed. Stress relaxation is the inverse of creep: a sample is held at a set length and the force it generates is measured [4].

A typical time-dependent material at constant load obtains the appearance in Figure 3.1 [5]. The curve can be divided into three regions. In the primary region the initial strains appears instantaneous with the load and the strain rate $(d\epsilon/dt)$ decreases. Even though the load is constant in the secondary region, the deformation continues to increase. The main part of the creep deformation occurs in the secondary region. Eventually, in the tertiary region, the strain rate increases until the material reaches the failure stress.

Creep can be modelled in different ways, for example, by the aid of viscoelasticity. However, another approach is to modelling creep-strains, i.e. summarize the elastic strain rate with the creep strain rate.

3.4. Viscoelasticity

The theory of viscoelasticity is suitable on bodies which both exhibit elastic and viscous effects, i.e. simultaneous storage of interior energy and dissipation at deformation [5]. When the deformation is irreversible, the mechanical energy supplied to the material, is transformed (dissipated) into heat [3]. Normally, the transformation requires a certain amount of time and cannot occur instantaneous, as a time-independent plastic deformation.
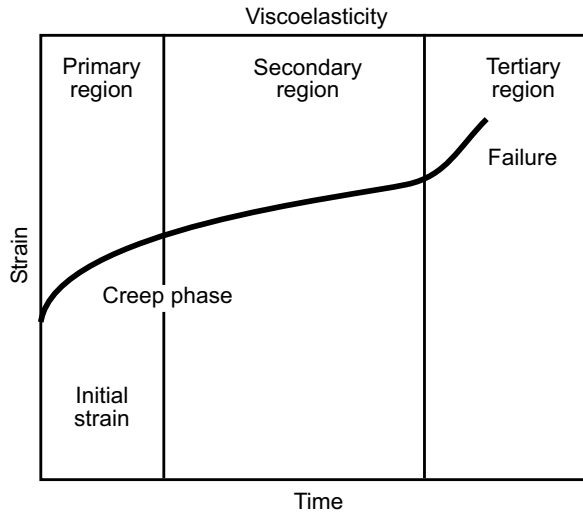
Figure 3.1: *A creep curve divided into three regions.*

If a material exhibits a combination of elastic and viscous behavior, the relation between stress and strain can not be prosperous described with material constants. Hence, the material behavior must be described by time-dependent material functions. At a general constitutive formulation, the stress becomes a functional of the strain, i.e. depending on the entire strain history. Thus, the stress at a given time is dependent on all previous moments [3].

At a certain time, the strain of a linear viscoelastic material increases linearly with the stress, contrary to a non-linear viscoelastic material, as presented in Figure 3.2 [6]. When the strains exceeds the proportional limit, the behavior becomes non-linear viscoelastic [8].

3.4.1. Maxwell and Kelvin-Voigt

To conveniently describe the viscoelastic material behavior, mechanical models are required. Hereby, the governing differential equations can be visualized. Even though these models occasionally yields a verbose description of the macroscopic material behavior, it is important to underline the models do not reflect the mechanism governing the molecular or atomic interaction [3].

The two simplest constitutive equations for modelling viscoelasticity are the Maxwell and the Kelvin-Voigt models. The mechanical properties of a material that exhibits linear viscoelasticity can be illustrated by a model consisting of a Hookean spring and a Newtonian dashpot, as shown in Figure 3.3.
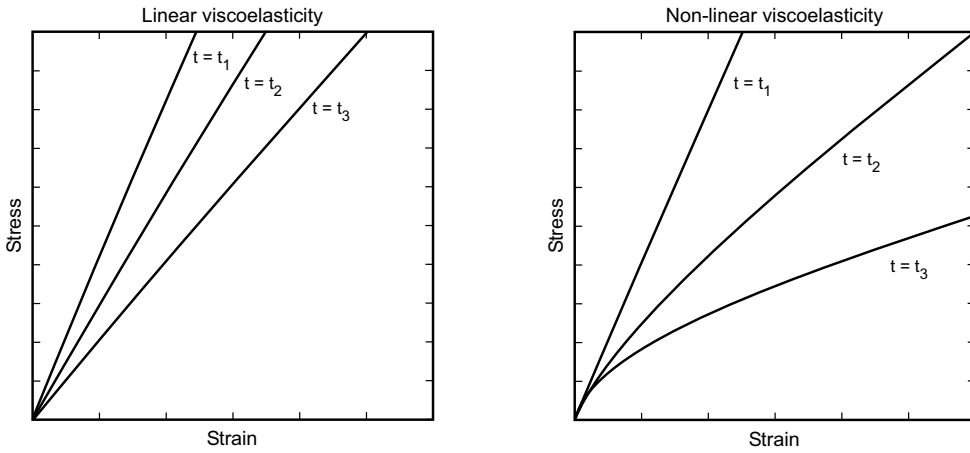
Figure 3.2: *Isochronous curves, a linear viscoelastic material to the left and a non-linear viscoelastic material to the right [6].*
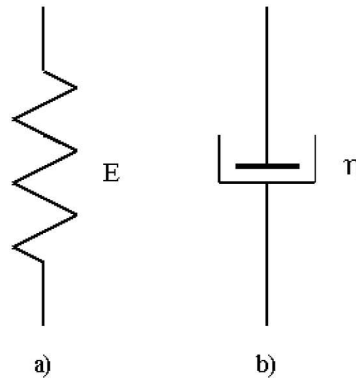
Figure 3.3: *(a) Spring with stiffness E, (b) damper with viscosity η.*

The established stress in the Hookean spring equals the modulus of elasticity multiplied by the elastic strain as

$$\sigma^e = E\epsilon^e \tag{3.6}$$

while in the Newtonian element, the stress equals the viscosity multiplied by the strain rate as

$$\sigma^v = \eta\dot{\epsilon}^v \tag{3.7}$$

where superscripts e and v denote the elastic and viscous behavior, respectively. Moreover, a dot denotes the time derivative, i.e. the strain rate $\dot{\epsilon}^v = d\epsilon^v/dt$ [7].

The combination of these two elements forms more complex mechanical models, which depict a viscoelastic material behavior. In this consistency, the Maxwell element is one of
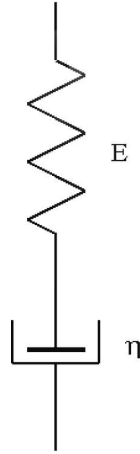
Figure 3.4: *A Maxwell element, consisting of a spring and a dashpot in series.*

the most ordinary models. Figure 3.4 depicts a single spring and a dashpot in series.

When two elements connected in series are loaded, they will obtain the same stress. To achieve the total strain, the strain in the spring and damper are summarized. Thus, a connection between the stress and strain is expressed

$$s\tilde{\epsilon}(s) = \mathcal{L}\left\{\frac{d\epsilon(t)}{dt}\right\} = \mathcal{L}\left\{\frac{1}{E}\frac{d\sigma(t)}{dt} + \frac{\sigma(t)}{\eta}\right\} = \left(\frac{s}{E} + \frac{1}{\eta}\right)\tilde{\sigma}(s) \qquad (3.8)$$

$$\Longleftrightarrow$$

$$\tilde{\epsilon}(s) = \left(\frac{1}{E} + \frac{1}{s\eta}\right)\tilde{\sigma}(s) \qquad (3.9)$$

Hence, the retardance for the Maxwell-element is obtained

$$\tilde{U}_M(s) = \frac{1}{E} + \frac{1}{s\eta} \qquad (3.10)$$

In a similar manner, the relaxance is displayed

$$\tilde{Q}_M(s) = \frac{E\tau_M s}{1 + \tau_M s} \qquad (3.11)$$

where the relaxation-time $\tau_M = \dfrac{\eta}{E}$ [3].

Apart from the Maxwell element, another simple model is the Kelvin-Voigt, shown in Figure 3.5, where the elements serve as a pair in parallel.
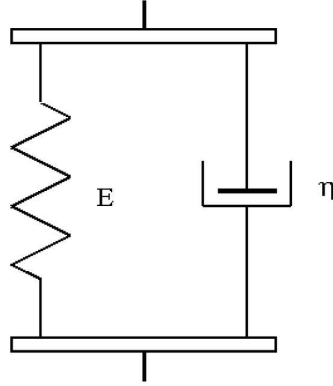
Figure 3.5: *A Kelvin-Voigt element consisting of a spring and a dashpot in parallel.*

When the system is loaded, the elements in pair obtain the same strain, whereas the total stress is the sum of the stress in the spring and the damper. Laplace transformation yields

$$\tilde{\sigma} = \mathcal{L}\{\sigma_s(t) + \sigma_d(t)\} = \mathcal{L}\left\{E\epsilon(t) + \eta\frac{d\epsilon(t)}{dt}\right\} = (E + \eta s)\tilde{\epsilon}(s) \qquad (3.12)$$

From the equation above, the relaxation of the Kelvin-Voigt element is obtained

$$\tilde{Q}_{kv}(s) = E + \eta s \qquad (3.13)$$

The retardation is given by

$$\tilde{U}_v(s) = \frac{1}{E(1 + \tau_v s)} \qquad (3.14)$$

where, the retardation time equals $\tau_v = \dfrac{\eta}{E}$ [3].

3.4.2. Isochronous and Isometric curves

Isochronous stress-strain curves and isometric stress-time curves can be obtained from creep curves at different stress levels. Isochronous curves are constructed from cross sections in the creep curves at different times, as shown in Figure 3.6 and isometric curves are made from cross sections at different strains, presented in Figure 3.7. These curves are very useful for characterizing the viscoelastic behavior of a material [8].

3.4.3. Stress and Relaxation

Stress relaxation is defined as the time-dependent reduction of stress at a constant strain. If a constant strain, ϵ_0 is applied to a specimen, we can investigate the decay of the stress $\sigma(t)$ over time, as displayed in Figure 3.8.
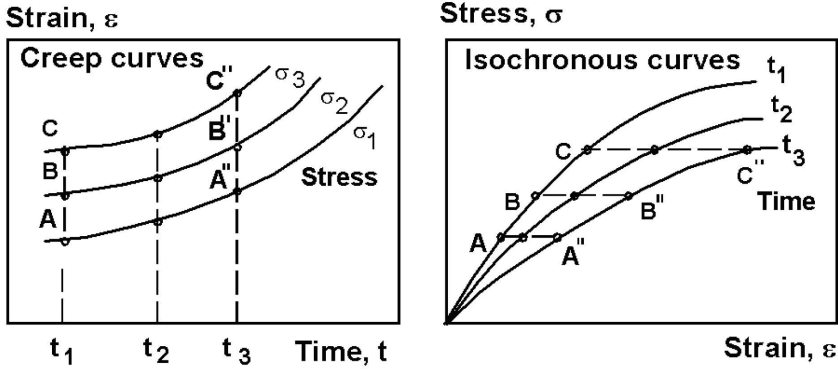
Figure 3.6: *Construction of isochronous curves from creep curves [8].*
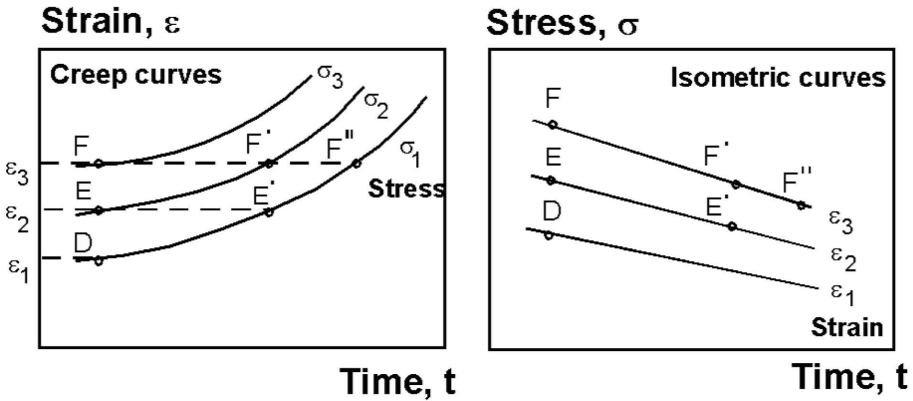
Figure 3.7: *Construction of isometric curves from creep curves [8].*

For a linear viscoelastic material, the stress relaxation modulus may conveniently be expressed as E(t)=$\sigma(t)/\epsilon$. In order to obtain an equilibrium value where the stress and the stress relaxation modulus are constant, i.e. $\sigma(t) \approx \sigma_\infty$ and E(t)$\approx E_\infty$, the material must be kept under strain for a sufficiently long time.

The relaxation curve can be described as a distribution of relaxation times. For a linear viscoelastic material, the relaxation modulus E(t), is expressed below in terms of a relaxation function $E(\tau)$

$$E(t) = E_\infty + \int_0^\infty E(\tau)e^{-t/\tau}d\tau \tag{3.15}$$

where τ is the relaxation time.
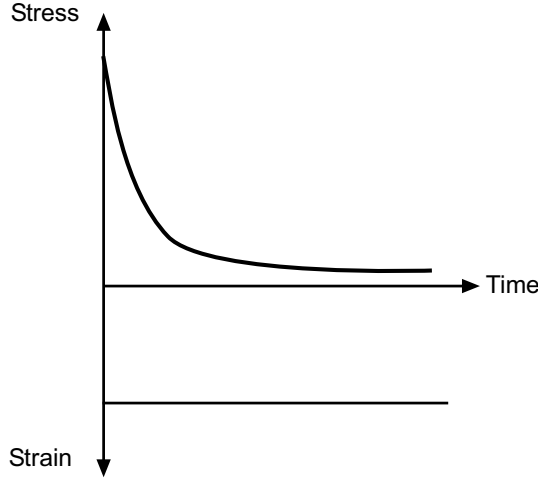
Figure 3.8: *Stress relaxation of a viscoelastic material. The strain is kept constant and the stress decays over time [8].*

We may facilitate the relaxation modulus through a Dirichlet series

$$E(t) = E_\infty + \sum_i E_i e^{-t/t_i} \tag{3.16}$$

where E_i and t_i are constants.

Since straining cannot be performed at infinite speed, it takes a certain time t_0 to reach the deformation during a relaxation experiment. If the strain is constant, the relaxation modulus is expressed by the relation

$$E(t) = E_\infty + \int_0^\infty E(\tau) e^{-t/\tau} \frac{\tau}{t_0} (e^{t_0/\tau} - 1) d\tau \tag{3.17}$$

where t is the total elapsed time [8].

3.4.4. Creep Curves

In order to give an illuminating exposition of an arbitrary creep curve for a polymeric material, the appearance in Figure 3.9 is considered. The rapid response of the initial deformation is displayed as the portion O to A in the creep curve, i.e. increment a. This is followed by a region of creep, A to B, where the strain rate decreases to a constant rate introduced in section B to C. Once the stress is removed, the instantaneous elastic response O to A is fully recovered from C to D, i.e. the distance a'=a. Then the curve drops from D to E in a slower recovery. However, this recovery is never completed, due to the initial state by the increment c'=c. This response is completely non-recoverable and a measure of the plastic flow [9].
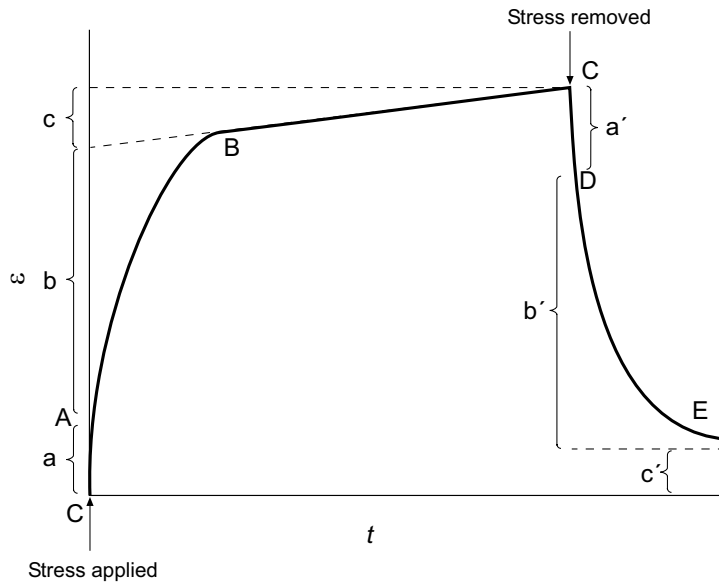
Figure 3.9: *The appearance of a creep curve: a, initial elastic response; b, region of creep; c, irrecoverable plastic flow [9].*

The elastic response reproduces the changes a and a' in Figure 3.9. A convenient element to model this response is the Hookean spring. The Kelvin-Voigt model corresponds to the changes b and b' in the region of creep. Eventually, a dashpot represent the plastic flow of the changes c and c'. To understand the appearance of the creep curve, the following mechanical models in Figure 3.10 may be useful.

The model is an assembly of a Maxwell element and a Kelvin-Voigt element, where the components of the latter are time-dependent. In Figure 3.10 (i) the system is at rest. When exposed to the stress σ, Figure 3.10 (ii), the spring E_1 of the system extends instantaneous to the amount of σ/E_1=a. Then, in Figure 3.10 (iii), the creep rate decreases with a gradually increase of load-carrying in the spring E_2, until it is completely extended and the dashpot η_2 no longer carries any load. As the spring E_2 now is fully extended, the creep rate switches to a constant phase, corresponding to the plastic flow in the dashpot η_3. The dashpot is deformed until the load is removed, illustrated in Figure 3.10 (iv). Now, the spring E_1 rapidly retreats (a') and the recoverable period ensues (b'). During this time, the dashpot η_2 is forced to retract to its initial position by the spring E_2. The position of the dashpot η_3 will remain in the extended state, since no spring can influence its position, Figure 3.10 (v). Thus, the non-recoverable plastic flow c'=$\sigma t/\eta_3$ is depicted by the dashpot η_3 [9].
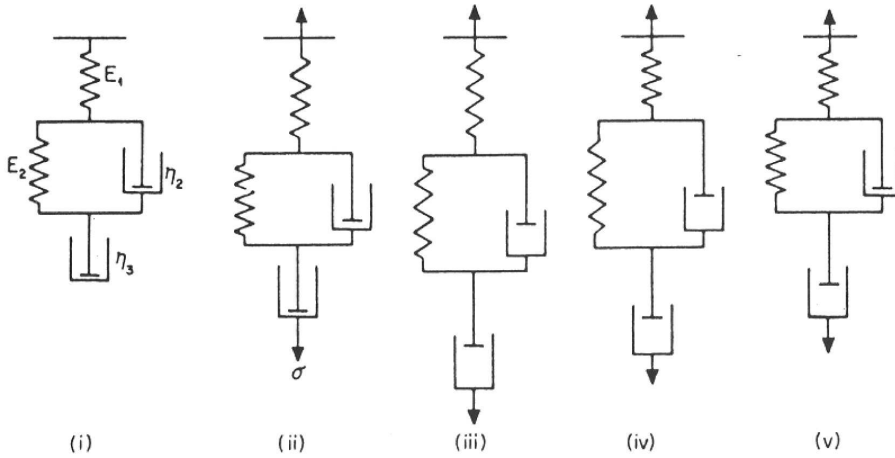
Figure 3.10: *Use of mechanical models to describe the creep behavior of a polymeric material [9].*

3.4.5. Boltzmanns Superposition Principle

The linearity in creep experiments can advantageously be expressed by the Boltzmann superpositions principle, which represents the linear viscoelastic behavior. Despite the application of stress or strain, which may cause a time-dependent response, each increment of stress or strain contributes to the final deformation. By simple addition of each contribution, the final deformation can be obtained [11]. An elementary derivation of Boltzmanns superpositions integral is

$$\epsilon(t) = \sigma_0 D(t) + (\sigma_1 - \sigma_0)D(t - u_1) + \ldots + (\sigma_i - \sigma_{i-1})D(t - u_i) \qquad (3.18)$$

where the quantity D(t), is the creep compliance defined as D(t)=ϵ(t)/σ, i.e. the transient strain per unit stress [12]. A more facilitated expression is

$$\epsilon(t) = \sum_{i=1}^{n} \sigma_i D(t - u_i) \qquad (3.19)$$

Equation (3.19) can in integral form be written as

$$\epsilon(t) = \int_{-\infty}^{t} \frac{\partial \sigma(u)}{\partial u} D(t - u) du \qquad (3.20)$$

In order to describe the creep compliance $D(t)$ of a linear viscoelastic material, the retardation function $D(\tau)$ may be established

$$D(t) = D_i + \int_{0}^{\infty} D(\tau)(1 - e^{-1/\tau})d\tau \qquad (3.21)$$

where τ is the retardation time and D_i is the instantaneous elastic compliance [8].

However, the following requirements must be fulfilled:

1. The compliance is independent of the applied stress.

2. The elongation due to a certain load is independent of the elongation due to a previous load [11].

3.4.6. Schapery's Model

To model non-linear viscoelastic creep, more advanced models must be utilized. The non-linear viscoelastic creep model for uniaxial loading derived by Schapery may be written

$$\epsilon(t) = g_0 A_0 \sigma + g_1 \int_0^t \Delta A \left(\psi - \psi'\right) \frac{dg_2\sigma}{d\tau} d\tau \tag{3.22}$$

where A_0 is the initial component and $\Delta A \left(\psi - \psi'\right)$ is the transient component of the linear viscoelastic creep compliance. The definition of the reduced time ψ is

$$\psi = \psi(t) = \int_0^t \frac{dt'}{a_\sigma} \tag{3.23}$$

and

$$\psi' = \psi(\tau) = \int_0^\tau \frac{dt'}{a_\sigma} \tag{3.24}$$

From the equations (3.22),(3.23), and (3.24) the parameters g_0, g_1, g_2, and a_σ are functions of the stress, σ. Moreover the material parameter a_σ is also a function of temperature and humidity [13]. For loading in the linear region, the material functions obtain a value of 1, according to Schapery. Thus, the Boltzmanns superpositions principle is employed [6]. In literature [14], it is shown that a creep model built on Schapery's theory, is well suited for small deformations in paper materials.

3.5. Modelling Creep-strains

Another way to modelling creep is to summarize the elastic strain rate with the creep strain rate, i.e.

$$\dot{\epsilon} = \dot{\epsilon}^e + \dot{\epsilon}^{cr} \tag{3.25}$$

In the FE-program ABAQUS, there are a number of creep models based on viscoelasticity. However, these cannot model the orthotropic behavior of paper.

A suitable model for isotropic or orthotropic creep is the power-law model, which is quite appealing for its simplicity. However, the range of application is restricted. The power-law creep model consists of two versions of hardening, namely time-hardening and strain-hardening. The first and simplest one is convenient when the applied load is constant. The strain-hardening version is suitable under fluctuating load. Moreover, relatively low stress holds for either version of the power-law.

If the achieved stress in the material widely exceeds the yield stress, the hyperbolic-sine creep law is applicable. However, if the load is cyclic, neither the power-law nor the hyperbolic-sine creep law are adequate [15].

3.5.1. Power-law Model

In the time-hardening form, the uniaxial equivalent creep strain rate $\dot{\tilde{\epsilon}}^{cr}$ depends on the uniaxial equivalent deviatoric stress $\tilde{q}$ and the total time t, i.e.

$$\dot{\tilde{\epsilon}}^{cr} = A\tilde{q}^n t^m \tag{3.26}$$

where A, n, and m are functions of the temperature, that need to be determined by experiment. For physically reasonable behavior, A and n, must be positive and $-1 < m \leq 0$. The value of A, may be very small for typical creep strain rates. However, if A is less than 10^{-27}, numerical difficulties can cause errors in the material calculations [15]. The parameters is presented in Tab. 3.1.

Table 3.1: *Example of numerical values fetched from the ABAQUS Online Documentation [15].*

	ABAQUS
A	$> 10^{-27}$
n	> 0
m	$-1 < m < 0$

The material is defined as isotropic or orthotropic. The parameter $\tilde{q}$, then corresponds to the Mises equivalent stress and the Hill's orthotropic deviatoric stress, respectively.

Since the load is constant and the stress is consistently less than the yield stress, the power-law model in the time-hardening form, is the most suitable for simulating paper of the creep laws available in ABAQUS. Therefore, no exposition is carried out of the other laws.

3.5.2. Orthotropic Creep

For materials that exhibit different creep behavior in different directions, orthotropic creep is applicable in conjunction with the *CREEP option. To be able to model orthotropic creep in ABAQUS, Hill's function is conveniently used

$$\tilde{q}(\sigma) = \sqrt{F(\sigma_{22} - \sigma_{33})^2 + G(\sigma_{33} - \sigma_{11})^2 + H(\sigma_{11} - \sigma_{22})^2 + \atop +2L\sigma_{23}^2 + 2M\sigma_{31}^2 + 2N\sigma_{12}^2} \tag{3.27}$$

where $\tilde{q}(\sigma)$ is the equivalent stress and F, G, H, L, M, and N, are constants extracted from experimental tests made in various directions of the material, defined as

$$\begin{aligned}
\text{F} &= \frac{1}{2}\left(\frac{1}{R_{22}^2} + \frac{1}{R_{33}^2} - \frac{1}{R_{11}^2}\right) \\
\text{G} &= \frac{1}{2}\left(\frac{1}{R_{33}^2} + \frac{1}{R_{11}^2} - \frac{1}{R_{22}^2}\right) \\
\text{H} &= \frac{1}{2}\left(\frac{1}{R_{11}^2} + \frac{1}{R_{22}^2} - \frac{1}{R_{33}^2}\right) \\
\text{L} &= \frac{3}{2R_{23}^2} \\
\text{M} &= \frac{3}{2R_{13}^2} \\
\text{N} &= \frac{3}{2R_{12}^2}
\end{aligned} \tag{3.28}$$

The variables R_{11}, R_{22}, R_{33}, R_{12}, R_{13}, and R_{23}, are orthotropic creep stress ratios, which the user must define in each direction [15]. However, the variables cannot be chosen arbitrarily. The yield surface in the deviatoric stress plane must be a closed surface. Thus, the following constraint is established.

$$\frac{4}{R_{11}^2 R_{22}^2} > \left[\frac{1}{R_{33}^2} - \left(\frac{1}{R_{11}^2} + \frac{1}{R_{22}^2}\right)\right]^2 \tag{3.29}$$

This inequality restricts the degree of orthotropy for which application of Hill's criterion is permissible [16].

To model orthotropic creep, the *POTENTIAL option in ABAQUS is used to specify the stress ratios appearing in Eq. (3.28). When the creep strain rates are the same in all directions, R_{ij} describes the quotients between the current stresses and the equivalent stress, i.e.

$$\begin{aligned}
R_{11} &= \frac{\sigma_{11}}{\tilde{q}}, & R_{22} &= \frac{\sigma_{22}}{\tilde{q}}, & R_{33} &= \frac{\sigma_{33}}{\tilde{q}}, \\
R_{12} &= \frac{\sigma_{12}}{\tilde{q}/\sqrt{3}}, & R_{13} &= \frac{\sigma_{13}}{\tilde{q}/\sqrt{3}}, & R_{23} &= \frac{\sigma_{23}}{\tilde{q}/\sqrt{3}}
\end{aligned} \tag{3.30}$$

The ratios are either constants or functions of the temperature. If the R_{ij} values are set to unity, isotropic creep is obtained [15].

3.5.3. Creep Models Available through Subroutines

A material model for simulating orthotropic creep behavior, is the model introduced in literature [17]. This model was originally made for describing creep in wood but may also be applicable on paper, since both paper and wood are fibrous orthotropic materials.

Based on the superpositions principle where each increment of stress contributes to the final deformation, see Boltzmann superpositions principle Eq. (3.19), the creep strain is given by

$$\bar{\epsilon}^{cr} = \int_0^t \bar{C}_c(t,t') \frac{d\bar{\sigma}(t')}{dt'} dt' \tag{3.31}$$

where $\bar{C}_c(t,t')$ is the creep compliance matrix for the orthotropic directions and $\bar{\sigma}(t')$ is the local stress vector. Consider a constant stress applied at the time t', i.e. $\sigma(t) = \sigma\Theta(t-t')$, Eq. (3.31) shows that the creep strain is proportional to the stress, because $\epsilon(t) = C_c(t')\sigma(t')$. A suitable definition of the relative creep is the ratio $\phi = \epsilon_c/\epsilon_e$, i.e. the quotient of the creep strain and the elastic strain. The step function $\phi(t-t')$ obtain a value of 1 when (t-t')≥0 and 0 when (t-t')<0. Hence, the creep compliance matrix $\bar{C}_c(t,t')$ for an orthotropic material takes the form

$$\bar{C}_c(t,t') = \begin{bmatrix} \frac{1}{E_l}\phi_{\sigma_l} & -\frac{\nu_{rl}}{E_r}\phi_{\nu_{rl}} & -\frac{\nu_{tl}}{E_t}\phi_{\nu_{tl}} & 0 & 0 & 0 \\ -\frac{\nu_{lr}}{E_l}\phi_{\nu_{lr}} & \frac{1}{E_r}\phi_{\sigma_r} & -\frac{\nu_{tr}}{E_t}\phi_{\nu_{tr}} & 0 & 0 & 0 \\ -\frac{\nu_{lt}}{E_l}\phi_{\nu_{lt}} & -\frac{\nu_{rt}}{E_r}\phi_{\nu_{rt}} & \frac{1}{E_t}\phi_{\sigma_t} & 0 & 0 & 0 \\ 0 & 0 & 0 & \frac{1}{G_{lr}}\phi_{\tau_{lr}} & 0 & 0 \\ 0 & 0 & 0 & 0 & \frac{1}{G_{lt}}\phi_{\tau_{lt}} & 0 \\ 0 & 0 & 0 & 0 & 0 & \frac{1}{G_{rt}}\phi_{\tau_{rt}} \end{bmatrix} \tag{3.32}$$

where the relative creep functions ϕ_{σ_l}, ϕ_{σ_r}, and ϕ_{σ_t}, depend on constant uniaxial tensile stress in the respective orthotropic directions. Further, $\phi_{\tau_{lr}}$, $\phi_{\tau_{lt}}$, and $\phi_{\tau_{rt}}$, correspond to the relative shear functions due to constant shear stress in respective orthotropic plane. Finally, $\phi_{\nu_{rl}}$, $\phi_{\nu_{lr}}$, $\phi_{\nu_{tl}}$, $\phi_{\nu_{lt}}$, $\phi_{\nu_{tr}}$, and $\phi_{\nu_{rt}}$, denote the relative Poisson's creep function due to uniaxial tensile stress in the respective orthogonal directions.

For plane stress considered, the compliance matrix $\bar{C}_c(t,t')$ can be reduced to

$$\bar{C}_c(t,t')_{ps} = \begin{bmatrix} \frac{1}{E_l}\phi_{\sigma_l} & -\frac{\nu_{rl}}{E_r}\phi_{\nu_{rl}} & 0 \\ -\frac{\nu_{lr}}{E_l}\phi_{\nu_{lr}} & \frac{1}{E_r}\phi_{\sigma_r} & 0 \\ 0 & 0 & \frac{1}{G_{lr}}\phi_{\tau_{lr}} \end{bmatrix} \tag{3.33}$$

Because the compliance matrix is symmetric, the requirement $\phi_{\nu_{rl}}=\phi_{\nu_{lr}}$, $\phi_{\nu_{tl}}=\phi_{\nu_{lt}}$, and $\phi_{\nu_{tr}}=\phi_{\nu_{rt}}$ must be fulfilled. This means when plane stress is adopted, four functions describe the viscoelastic behavior. These functions must be calibrated by experiment.

4. Material Behavior of Paper and Polymers

4.1. General Remarks

In order to formulate a suitable FE-model, based on creep, a profound knowledge of the material behavior of the various materials in a beverage package is required.

This chapter presents an overview of the laminate structure, material directions, and mechanical properties of paper and polymers.

4.2. Paper

Paper is a bonded, layered network of randomly arranged short fibers lying mainly in the plane of the sheet [18]. The average length of the fibres exceeds the thickness of the web, which results in a more or less pronounced two-dimensional network. Paper may be considered as a homogenous multiphase composite, comprised of fibres, moisture, voids, and chemical additives [14].

The material behavior of paper is to a large extent anisotropic, i.e. the material exhibit various properties of the principal directions of paper. With three orthogonal symmetric planes, the paper material is designated as orthotropic.

In comparison to the MD, the tensile stiffness in the CD is half of the stiffness, and in the ZD the magnitude is commonly two orders lower than in the MD [14]. In Figure 4.1, the mutual relationship of MD and CD is shown. At the same stress level, the creep-rate of paper is considerably higher in the CD than in the MD.

The behavior of paper may be considered as linear and orthotropic in the elastic region. To describe the linear elastic behavior of paper, the following assumptions are made [19]

1. The material is homogenous and uniform.

2. The material is orthotropic.

An orthotropic material consists of three symmetrical planes with differing material prop-
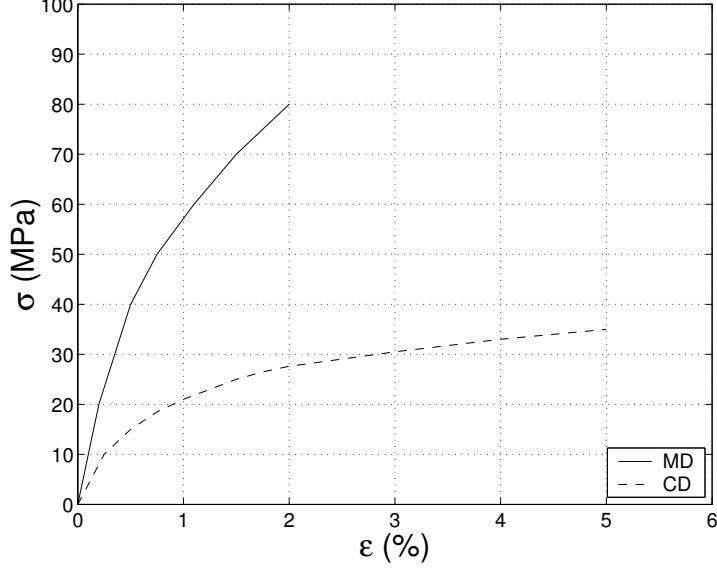
Figure 4.1: *Stress-strain curves for paper in MD and CD [14].*

erties. Hooke's law, Eq. (3.3), for an orthotropic material becomes

$$
\begin{bmatrix} \epsilon_{11} \\ \epsilon_{22} \\ \epsilon_{33} \\ \gamma_{23} \\ \gamma_{13} \\ \gamma_{12} \end{bmatrix} = \begin{bmatrix} \frac{1}{E_1} & -\frac{\nu_{21}}{E_2} & -\frac{\nu_{31}}{E_3} & 0 & 0 & 0 \\ -\frac{\nu_{12}}{E_1} & \frac{1}{E_2} & -\frac{\nu_{32}}{E_3} & 0 & 0 & 0 \\ -\frac{\nu_{13}}{E_1} & -\frac{\nu_{23}}{E_2} & \frac{1}{E_3} & 0 & 0 & 0 \\ 0 & 0 & 0 & \frac{1}{G_{23}} & 0 & 0 \\ 0 & 0 & 0 & 0 & \frac{1}{G_{13}} & 0 \\ 0 & 0 & 0 & 0 & 0 & \frac{1}{G_{23}} \end{bmatrix} \begin{bmatrix} \sigma_{11} \\ \sigma_{22} \\ \sigma_{33} \\ \tau_{23} \\ \tau_{13} \\ \tau_{12} \end{bmatrix}
\tag{4.1}
$$

where the normal strains ϵ and the shear strains γ, relates to the normal stresses σ and the shear stresses τ. However, it can be shown that this matrix is symmetric, if the strain energy is independent of the loading path. Symmetry emerges when

$$
\frac{\nu_{21}}{E_2} = \frac{\nu_{12}}{E_1}; \quad \frac{\nu_{31}}{E_3} = \frac{\nu_{13}}{E_1}; \quad \frac{\nu_{32}}{E_3} = \frac{\nu_{23}}{E_2}
\tag{4.2}
$$

The in-plane parameters describe the behavior in the MD-CD-plane and ZD is the out-of-plane direction. In this study, the index 1 denotes the MD, index 2 denotes the CD and the index 3 denotes ZD. Consider a material exposed to an uniaxial stress state, $\sigma_{11} \neq 0$, then the following is obtained

$$
\frac{\epsilon_{22}}{\epsilon_{11}} = -\nu_{12} \qquad \frac{\epsilon_{33}}{\epsilon_{11}} = -\nu_{13}
\tag{4.3}
$$

and similar for $\sigma_{22} \neq 0$

$$
\frac{\epsilon_{11}}{\epsilon_{22}} = -\nu_{21} \qquad \frac{\epsilon_{33}}{\epsilon_{22}} = -\nu_{23}
\tag{4.4}
$$

while for $\sigma_{33} \neq 0$

$$\frac{\epsilon_{11}}{\epsilon_{33}} = -\nu_{31} \qquad \frac{\epsilon_{22}}{\epsilon_{33}} = -\nu_{32} \qquad (4.5)$$

In order to calculate Poisson's ratios, these relations are useful. However, these equations are general and do not require symmetry of the **D** matrix [19].

4.2.1. Mechanical Properties of Paper

In accordance with other polymerical materials, the mechanical properties of paper are strongly moisture- and time-dependent. For an increase in moisture content the elastic stiffness reduces markedly. The time-dependency results in viscoelasticity, and creep, and in combination of moisture changes, mechano-sorptive creep. The time-dependent material behavior of paper, generally demands a non-linear constitutive model. Despite the absence of an established theory of non-linear material behavior, several models built on linear pure viscoelastic assumptions have been suggested. In numerous studies, it has been shown that many cellulosic materials have a non-elastic viscoelastic behavior. The interaction of load and moisture content in paper can cause many practical problems, even under constant load [20].

4.2.2. Mechano-Sorptive Creeping

Paper exposed to a variable relative humidity and to a constant load, exhibits an accelerated creep. This phenomena is called mechano-sorptive creep. The mechanical response of paper, due to loading, differs substantially from a constant relative humidity environment, to a cycled relative humidity climate.

The results of three tensile creep tests, tested with equal loading and various moisture conditions, are shown in Figure 4.2.

The first test was made at a constant moisture level of 30% RH, the second at a constant moisture level of 90% RH, and the third, the RH was cycled between 30% and 90%, at a rate of 1% RH/min through four full cycles. In the latter, the load was applied at the initiation of cycling. In Figure 4.2, the acceleration in creep, due to the variation in relative humidity, is shown together with the creep curves for constant moisture conditions [20].

4.3. Polymer

Polymers are either synthetic or natural, usually organic substances, which are built up by chains of molecules. These consist of smaller molecules called monomers [21].
A polymeric material is in most cases either amorphous or partly crystalline. For low temperatures, amorphous polymers, constitued of plastic, are vitreous and the chains immobile. When heating an amorphous polymer to glass transition temperature T_g, the
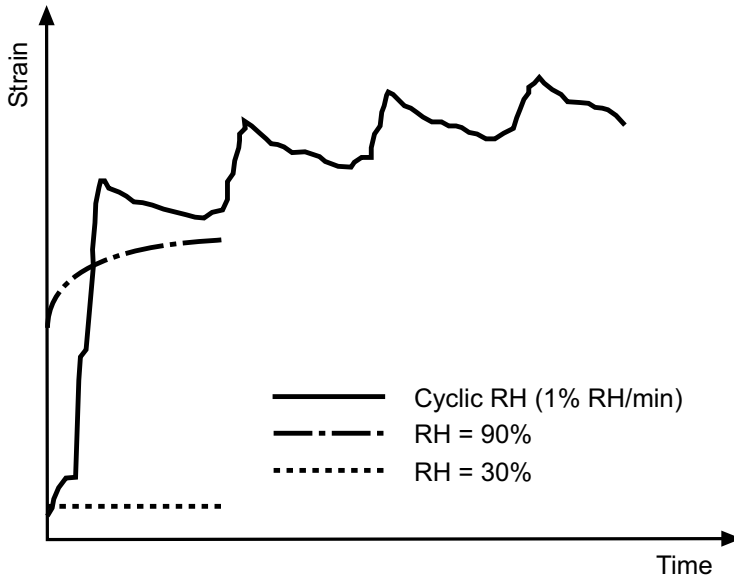
Figure 4.2: *Moisture accelerated creep under a variable relative humidity [20].*

chains begin to coordinate large-scale motions and after a time, the polymer (the plastic) turns viscous and formable. The material behavior of polymers is isotropic, i.e. the properties are the same in all directions. Thus, the material parameters ν and E are sufficient to describe the constitutive relations.

In Figure 4.3, a typical stress-strain curve for a polymeric material is shown. In the linear region, the material behavior is linear elastic and in the non-linear region, the material turns plastic and eventually, reaches the failure stress.

With a pronounced temperature-dependent behavior, the polymers become less brittle with the increase of temperature [4]. Further, as the temperature increases, the elongation generally increase, whereas both the yield strength and rigidity decrease [9].

4.3.1. Mechanical Properties of Polymers

Polymers generally possess a viscoelastic behavior, i.e. the mechanical properties are time-dependent. Neither the Maxwell or the Kelvin-Voigt model alone can reproduce the creep behavior of polymers. Instead, a proper model is the four-element model shown in Figure 3.10.
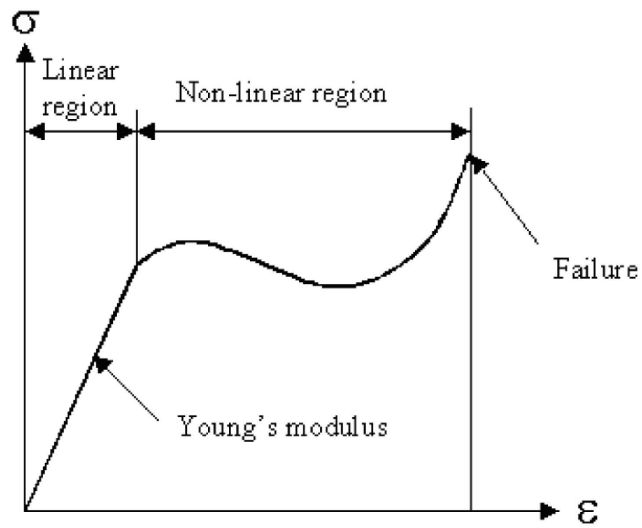
Figure 4.3: *Generalized stress-strain curve for polymerical material [4].*

5. Material Characterization

5.1. General Remarks

This chapter presents a survey of the various experiments needed to develop a suitable FE-model, for simulation of bulging. The tests performed in this study, determined the modulus of elasticity of paper, and, creep tests of paper, laminate (the package material), aluminium, and polymers were carried out. Further, the stiffness and residual moment of the creases were determined by experiment, and finally, a bulge test determining the change in shape of a package was performed, used as a verification model.

Only tensile creep tests were performed on the materials. Since the stored package is subjected to forces from the internal pressure of the liquid only, creep due to compressive forces was neglected in the tests. However, creep due to shearing forces may develop in the package, but was not tested experimentally.

During the performed literature study of creep in paper and plastics, it was hard to find other sources of information, regarding tensile creep test. Therefore, experimental tests were performed at the Div. of Structural Mechanics, LTH. However, some of the experimental tests presented in this study were obtained from Tetra Paks study of creep at SP Borås.

5.2. Determination of the Modulus of Elasticity in Paper

Two different methods, Alwetron and Instron were utilized to determine the modulus of elasticity (MOE). The method-Alwetron gives merely a value of the MOE, therefore, method-Instron is needed to obtain a complete stress-strain curve.

5.2.1. Experimental Method-Alwetron

All tests, according to method-Alwetron, were performed in the Paper Laboratory at Tetra Pak. To determine the modulus of elasticity of paper, a standardized test method used by Tetra Pak was employed. In this method, the paper specimens were mounted to a tensile-strength machine, manufactured by Alwetron TH1, displayed in Figure 5.1. Further, 10 specimens were cut out from each of the MD- and CD-direction with a length of 140 mm and a width of 15 mm from several sheets of paper, (taken from various parts of the paper-roll). Before cutting out the samples, the paper were dried for 30 minutes in an oven and then stabilized at the ambient climate of 23°C and RH 50%. To include the

Figure 5.1: *The tensile testing machine.*

variation of the material behavior, the specimens were sampled from various locations of
the paper-roll. The specimens were tested at a constant strain rate of 10 mm/min in MD
and 20 mm/min in CD, until failure occurred.

5.2.2. Results

The result data from the machine was based on stiffness per meter and to determine the
MOE, the results were divided by the thickness of the paper. The average thickness was
determined to 0.395 mm by the L&W Micrometer 51 device, shown in Figure 5.2. The
modulus of elasticity was determined as mean values of ten tests in each direction to 5121
MPa in MD and to 2670 MPa in CD.

5.2.3. Experimental Method-Instron

The complete stress-strain curve of the paper material, was not available by using the
Alwetron tensile test machine. Therefore, a uniaxial tensile test was performed to obtain
the full stress-strain curve by aid of an Instron 4400R device, shown in Figure 5.3.

Specimens with a width of 15 mm and a length of 140 mm were tested in uniaxial stress-
state at a strain rate of 1 mm/min. The paper strips were loaded to failure. For each
material direction, one test was made and the obtained curves are shown in Figure 5.4
and Figure 5.5.

Figure 5.2: *Thickness measurement device L&W Micrometer 51.*

Figure 5.3: *A uniaxial tensile test set-up in an Instron 4400R device.*

5.2.4. Results

On the basis of the force-displacement curves, the MOE can be determined, from the initial slope of the curve in the elastic region. Further, the stress was calculated as the imposed load divided by the area of the cross-section and the strain as the displacement of the load cell divided by the initial length. The MOE was determined in this way in MD to 3353 MPa and to 1434 MPa in CD. These values are considerable lower in
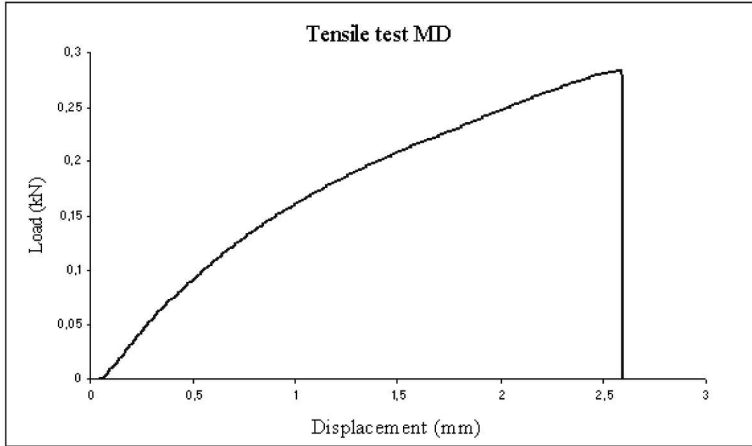
Figure 5.4: *Displacement versus load in MD determined by use of the Instron 4400R device.*
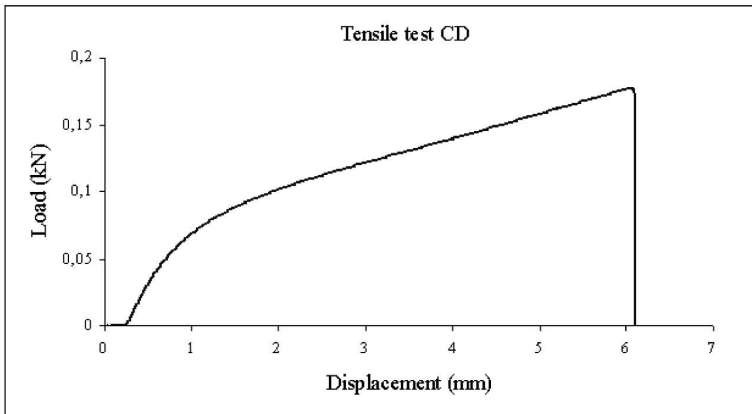
Figure 5.5: *Displacement versus load in CD determined by use of the Instron 4400R device.*

comparison to the values determined in method-Alwetron. In comparison to previous test result in literature [19], the higher values of the modulus of elasticity, as determined by method-Alwetron, are assumed to give more accurate values.

5.2.5. Summary

An comparison of the modulus of elasticity determined by the method-Alwetron and the method-Instron, is shown in Tab. 5.1.

Table 5.1: *The modulus of elasticity as determined by the method-Alwetron and the method-Instron, respectively.*

Material direction	Method-Alwetron	Method-Instron
MD [MPa]	5121	3353
CD [MPa]	2670	1434

5.3. Determination of the Creep Behavior of Paper

5.3.1. Experimental Method

Strips of paper were cut out from sheets, taken from various parts of a large paper-roll. The width of the paper strips were 10 mm and the fixed length was set to 120 mm. The specimens were placed in a controlled climate at 23°C and RH 50%. As the mass of the paper strips varies with the moisture content, the specimens were weighed at certain intervals, to determine whether the specimens were in equilibrium with the ambient climate.

In order to get a picture of the variability in creep of the paper material, at least two tests at each load-level were performed, in the MD- and CD-directions, respectively. To determine the stress dependence of the creep rate, the specimens were exposed to a stress-level of 5-10 MPa, defined by Tetra Pak. Therefore, the corresponding load-levels were 20 N, 40 N, and 50 N. The load-levels correspond to the stress-levels of 5 MPa, 10 MPa, and 12.5 MPa, respectively.

As can be seen in Figure 5.6, the strips were clamped in the upper end, while the other end was loaded with weights of 2 kg, 4 kg, or 5 kg. The fixing was made with sand paper glued to the inside of two brackets, clamping the specimen. The weight, was lying on a dial gauge, which registered the displacement of the specimen. To prevent the weight from pendulate, a tiny hole was drilled in the weight, where the top of the dial gauge was inserted. Before loading, strings were mounted between a crane and the weight to keep it still and to prevent the specimen from being loaded. The loading was made by simply lowering the crane. The specimens were allowed to creep for two weeks and the dial gauge was read periodically, frequently in the beginning and more rarely in the end, due to the logarithmic behavior of the creep.

5.3.2. Results

The measurement results are shown in Figure 5.7 and Figure 5.8. The graph labelled TP, was obtained data from Tetra Pak, the other curves were performed at LTH. Further, the stress-levels of 12.5 MPa, 10 MPa, and 5 MPA correspond to the loads of 50 N, 40 N, and 20 N, respectively.

For tests with low creep rate, the influence of the sources of error becomes more noticeable. The discrepancy of the 10 MPa creep curves shown in Figure 5.7, depends likely on the variable material behavior of paper. It hardly seems probable that the paper strip

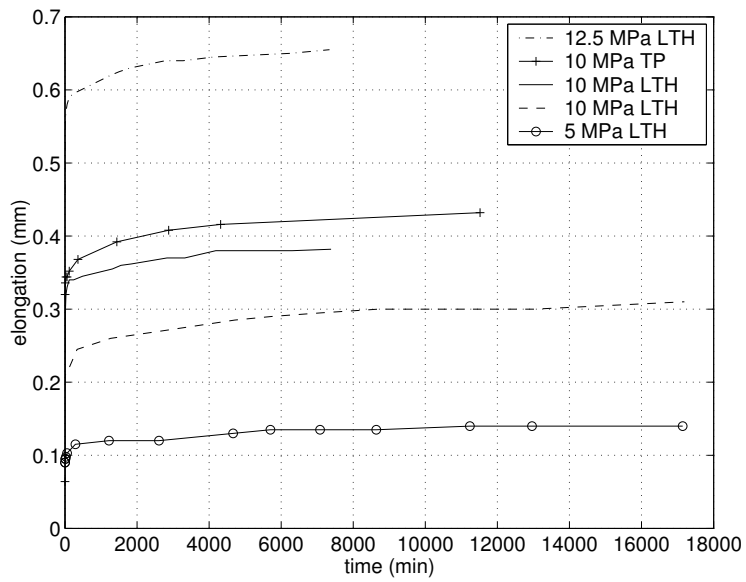Figure 5.6: *Creep test set-up of paper.*

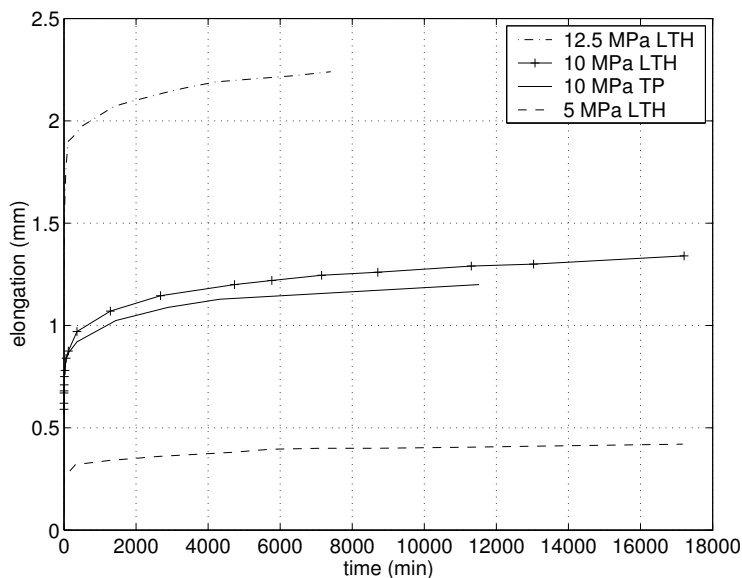Figure 5.7: *Results of creep tests of paper in MD.*

Figure 5.8: *Results of creep tests of paper in CD.*

has slipped in the fixing. The elapsed time of the various creep experiment varies, due to external circumstances.

It is of great interest to know how the paper is creeping. Therefore, the elastic part is withdrawn from the creep curves shown in Figure 5.9 and 5.10. An increase of the load-level varies non-linearly with the creep deformation. An increase from 5 MPa to 10 MPa, results in double the creep deformation in MD. In CD, an increase from 5-10 MPa gives a creep deformation more than three times larger. The creep deformation is approximately four to six times larger in CD, than in MD.

5.4. Determination of the Creep Behavior of Laminate

5.4.1. Experimental method

Similar to the tests made on plain paper, creep tests were carried out for the entire laminate in Figure 2.3. The load-levels of 40 N and 50 N, correspond to the stress-levels of 10 MPa and 12.5 MPa, respectively.

Unlike the creep tests of paper, four laminate strips were allowed to creep for six weeks, instead of two weeks.
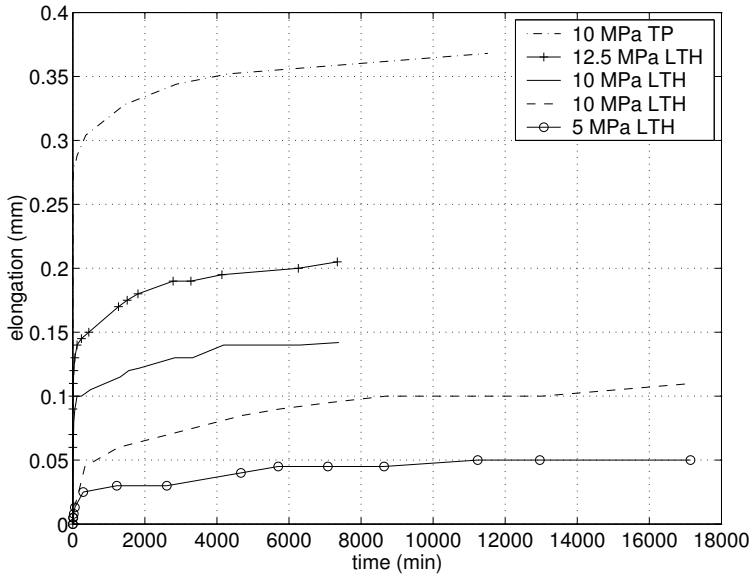
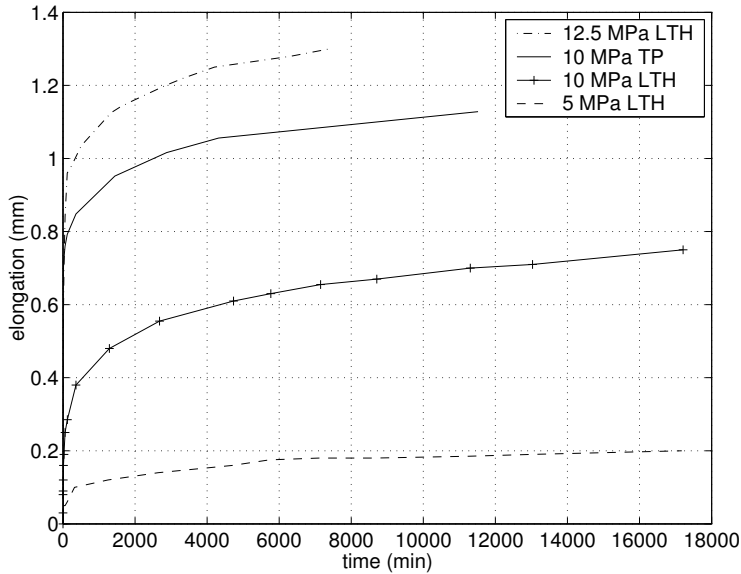Figure 5.9: *Creep of paper in MD without the elastic part.*

Figure 5.10: *Creep of paper in CD without the elastic part.*

5.4.2. Results

In Figure 5.11 and 5.12, it is obvious that an increase of the load varies non-linearly with the elastic + creep deformation. The elastic + creep deformation is approximately three
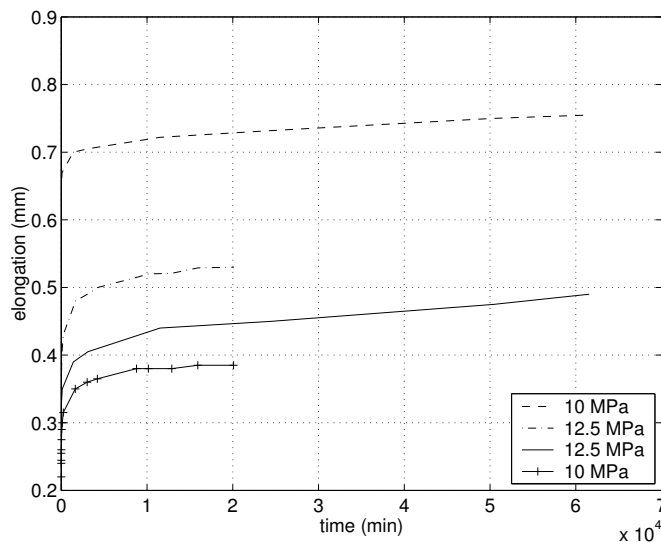
Figure 5.11: *Results of creep tests of laminate in MD.*

times larger in CD, in comparison to MD. Further, an increase from 10 MPa to 12.5 MPa, corresponds to an increase of 60 % of the elastic + creep deformation in CD. In MD, that kind of comparison is useless, due to the 10 MPa curve on top, which probably is caused by the material spreading or some errors made in the measurement. Within this thesis, there is no room for an investigation of the possible sources of error. Therefore, the results are not ignored.

5.5. Determination of Creep Behavior of Aluminium

Although the aluminium layer in the laminate is very thin, it contributes significantly to the overall stiffness, due to its high modulus of elasticity. The creep of the laminate, compared to plain paper, may be reduced if the creep of the aluminium is low. In order to consider the creep of aluminium, the time-dependent deformation must be experimentally determined. Due to the experimental cost, only two tests could be performed.

5.5.1. Experimental Method

The creep tests of aluminium was made similar to the tests made on paper and laminate, described in Section 5.3 and 5.4. Strips from an aluminium foil were cut out with a width of 20 mm. However, the thickness of 9 μm used in the laminate, was too thin and difficult to handle, therefore, a 14 μm foil was utilized. Instead of using weights, the specimen was mounted in to a MTS (Material Test System) uniaxial tensile device, in the Structural Mechanics laboratory, shown in Figure 5.13.
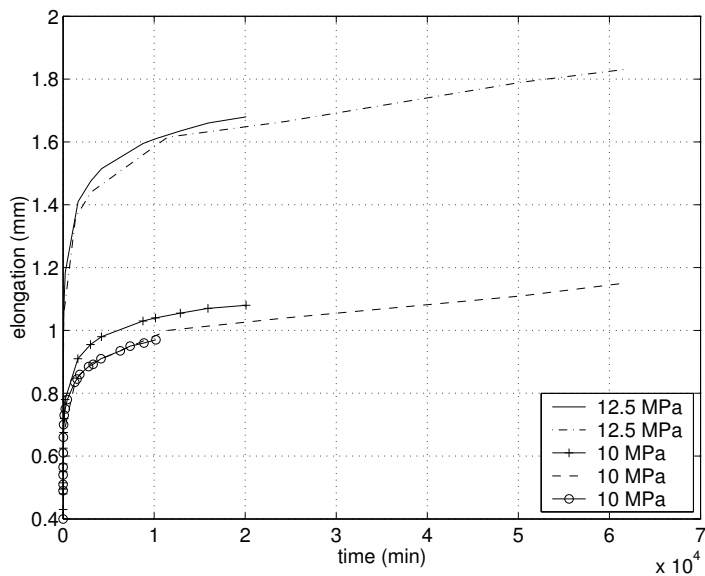
Figure 5.12: *Results of creep tests of laminate in CD.*

The free measuring length was approximately 140 mm and the test was made with two load levels of 14 N and 20 N, corresponding to 50 MPa and 71 MPa, respectively. As the aluminium is highly temperature-sensitive with a coefficient of linear heat expansion

Figure 5.13: *Creep test set-up of aluminium in a MTS.*
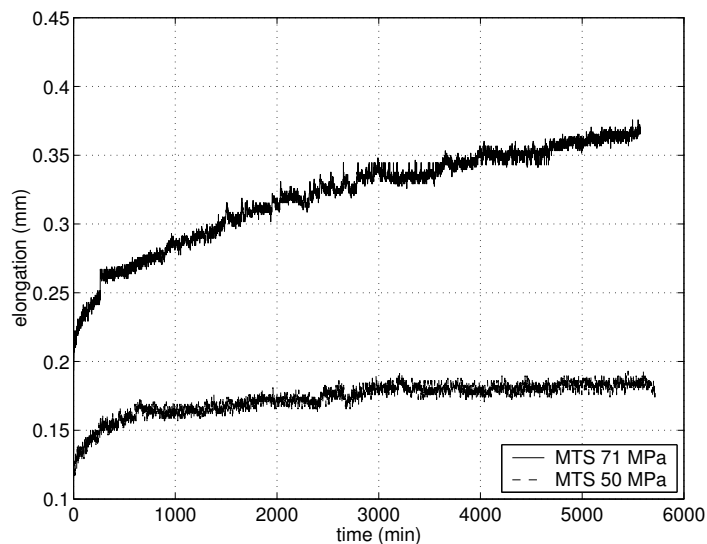
Figure 5.14: *Creep of aluminium, at the load-levels of 14 N and 20 N.*

of $2.4 \cdot 10^{-5}/K$, the ambient climate in the testing room was stabilized at 23°C and RH 50%. The load cell and the piston position sensor was connected to a computer, which registered the time, the displacement, and the load.

5.5.2. Results

The following creep curves shown in Figure 5.14 were obtained. Due to a break of the MTS, a perturbation of the 71 MPa graph occurred.

An increase of the stress-level of 50 MPa to 71 MPa, results in double the elastic + creep deformation. Therefore, it can be stated that the increase of the load varies non-linearly with the elastic + creep deformation. Moreover, the higher the stress, the slower the curvature.

5.6. Determination of the Creep Behavior of Polymer

5.6.1. Experimental Method

A tensile-test device DMA 2980 shown in Figure 5.15, was used for the determination of the creep behavior of the polymer, found in the top of the package. DMA stands for Dynamic Mechanical Analyzer. The tests were performed in the Polymer Laboratory at Tetra Pak R&D AB.

Figure 5.15: *The DMA 2980 testing machine.*

In Figure 5.16, a specimen of the polymer HDPE (High Density Polyethylene) material with a thickness of 0.325 mm, a width of 6.3 mm and a free length of 9.9 mm is shown. The specimens were exposed to an arbitrary chosen constant load of either 10 N or 18 N, corresponding to 4.5 MPa and 8 MPa, respectively. For each load-level, two experiments were performed.
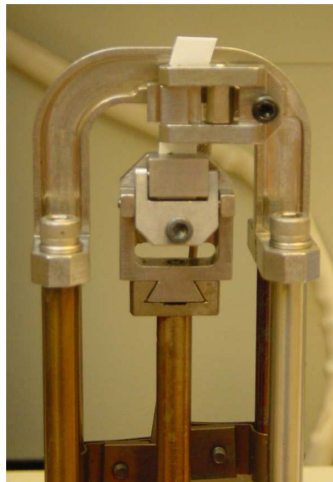

Figure 5.16: *A HDPE specimen clamped in the DMA testing machine.*
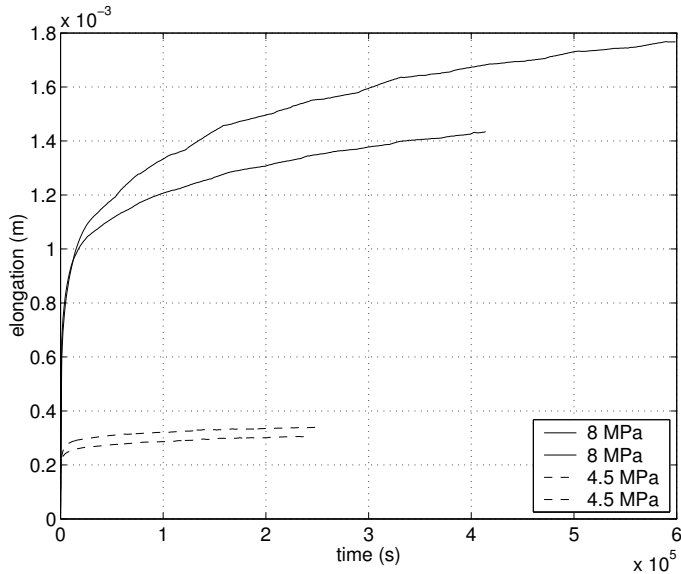
Figure 5.17: *Creep tests of polymer, performed by a tensile test device DMA 2980, at a constant load of either 10 N or 18 N over time.*

5.6.2. Results

In Figure 5.17, the creep of the polymer is presented. The elapsed time of the tests performed, varies due to limited access to the DMA 2980 device. The 10 N tests were allowed to creep for approximately three days and the 18 N tests for about six days. The variability of the curves might be caused by gliding in the fixing, the variable material behavior of the polymer, or the fact that the thickness of the specimens varied (0.310-0.330 mm).

An increase of the stress-level of 4.5 MPa to 8 MPa, increases the elastic + creep deformation by a factor of four to six. The higher the load, the slower the curvature.

5.7. Determination of the Residual Moment of Creases

5.7.1. Experimental Method

To model the behavior of the creases in a package, the stiffness and the residual moment of the creases need to be determined. The residual moment, i.e. the moment that remains in the material after the manufacturing of the package.

Strips of 25 mm in width were cut out from a sheet of laminate, which contained a number of creases. The laminate was stabilized at 23°C and RH 50%. A special device of the type Lorentzen & Wettre Creasability Tester PTS in the Paper Laboratory at Tetra Pak R&D AB, was used to determine the residual moment, displayed in Figure 5.18.

Figure 5.18: *The Lorentzen & Wettre Creasability Tester.*

The angle of the creases in the package of consideration is 45°, the laminate was therefore tested for this bending angle, shown in Figure 5.19.

The strips were clamped adjacent to a crease and 10 mm from the clamp, a load cell prevented the laminate from rotating with the clamp. The strip was initially bent to 45°, where it remained loaded for 50 sec, and then un-loaded and re-loaded, as shown in Figure 5.20.

5.7.2. Results

The laminate strips were bent, and the force and rotational angle were registered by a computer, which calculated the residual moment. The obtained results from the two tests, are shown in Figure 5.20.

5.8. Bulge Test

In Figure 1.1 on page 1, the appearance of the bulging phenomena is shown. In the bulge test, the change in length and width, along the height, of a package were studied over a period of time.

5.8.1. Experimental Method

To be convinced the package always would be correctly placed, a customized holding fixture was made. The fixture was surrounded by four laser devices, working in pair. One group determined the width of the package and the other group determined the length. In
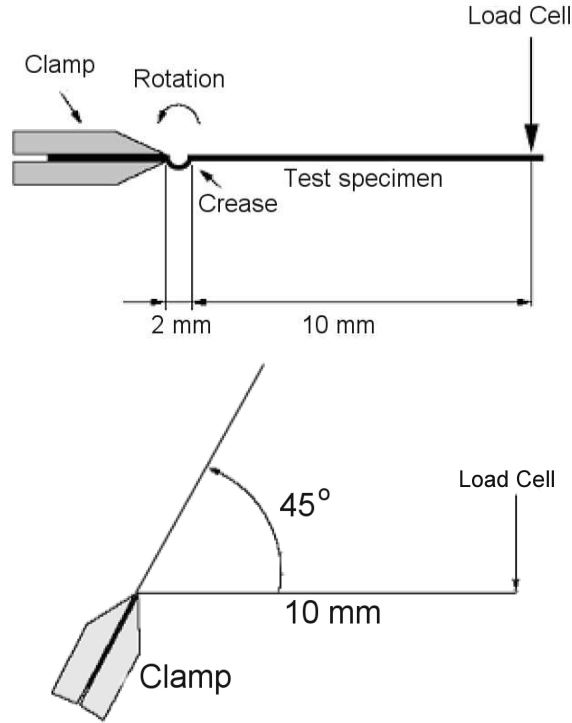
Figure 5.19: *Schematic drawing of the bending test of creases.*

order to measure length or width along the height, one of the laser devices determined the distance to the front of the package and the opposite laser device measured the distance to the backside. Thus, the length and width were determined by a computer for the entire height of the package.

To show the effects of bulging, bulge tests were performed at different times. Five packages were included to the test. Each package was initially measured empty as a reference, then the packages were filled and measured periodically, frequently in the beginning and more rarely in the end, due to the logarithmic behavior of the creep.

5.8.2. Results

Due to the geometry of the specific package, the measurement of the length is too insecure and therefore, only the width of the package is presented.

In Figure 5.21, the result of the bulge test is displayed. Each curve is actually a mean-value curve of five bulge tests. The width is the distance from an imagined centre line,
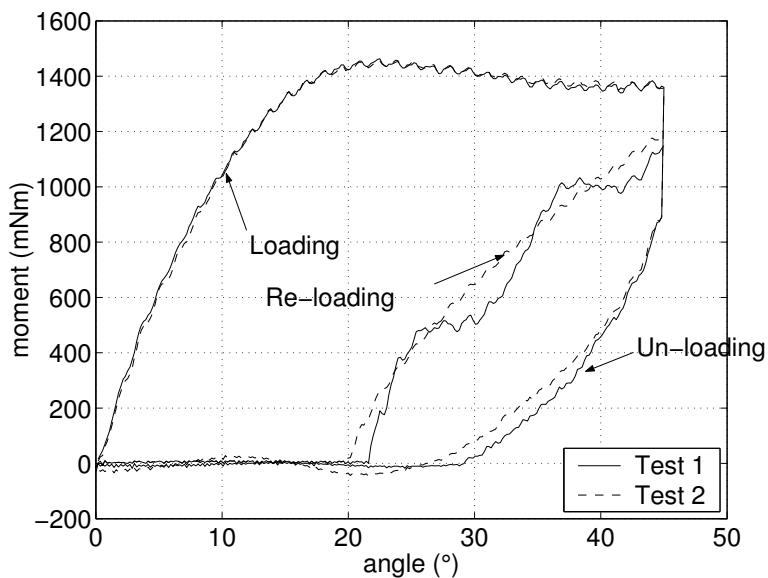
Figure 5.20: *The moment versus bending angle of a crease, exposed to loading, un-loading, and re-loading.*

which splits the entire package in half and the height is the vertical distance.

Of the result in Figure 5.22, one specific point of the package is considered. The bulging in this point is displayed over time. The point is located at an altitude of 100 mm, from the bottom of the package.
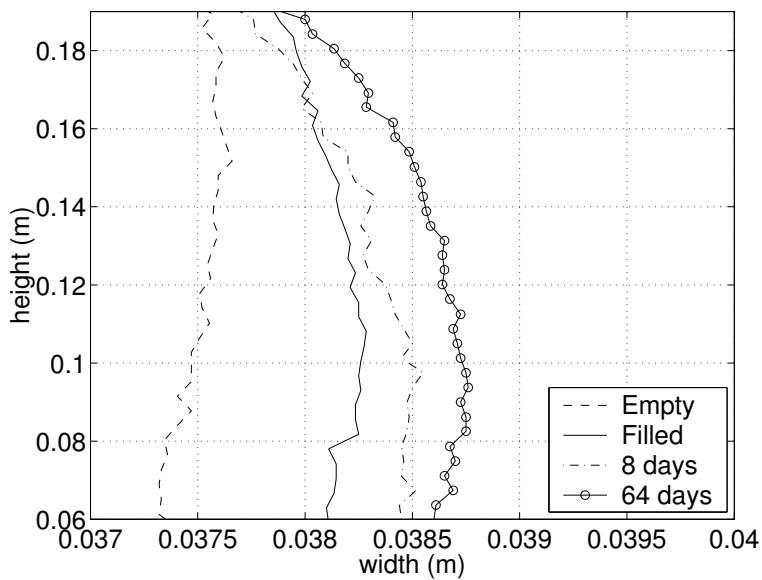
Figure 5.21: *Bulging along the height for the specific package.*
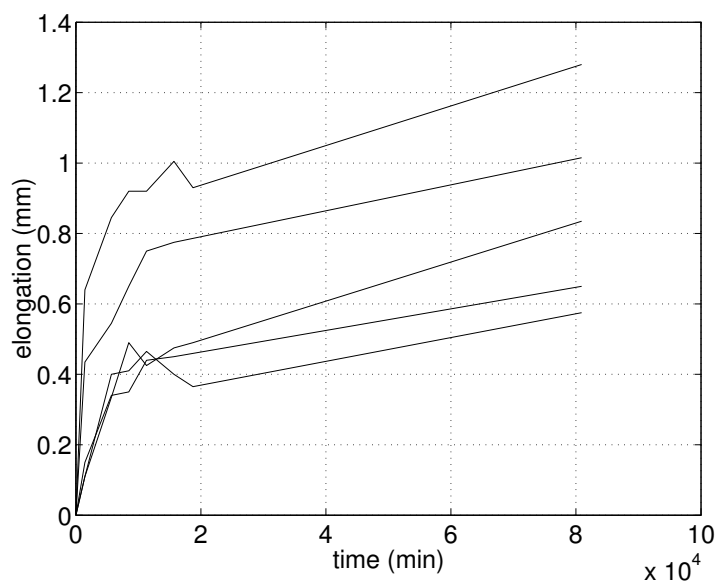
Figure 5.22: *Bulging at the center of five packages.*

6. Constitutive Models for Simulation of Creep in Packages

6.1. General Remarks

The essence of this master's thesis is to produce a resemblance of the experimental data to the constitutive models. To form the basis of the establishment of a more refined model, it is convenient to start with simple FE-models.

In this chapter a parameter study of a creep model is performed. Further, fitting of the parameters of this creep model to experimental data is carried out for a number of materials. But first and foremost, the model chosen for creep simulations is presented.

6.2. Model Chosen for Creep Simulations

When choosing a model, the specific case must me studied. In this study, the modelling is restricted to a constant temperature at 23°C and a humidity of 50% RH. No consideration is taken to the moisture content variation of the material, nor the fact that cyclic relative humidity cause accelerated creep.

The material properties of paper are orthotropic, i.e. different behavior in MD, CD, and ZD. Unlike paper, the material properties of aluminium and plastic are isotropic. Further, the load-levels of the simulations is held constant, in order to correspond to the constant loading conditions of the experimental tests.

Due to the constant loading conditions, the Power-law creep model with time-hardening was chosen in the simulations. The Power-law model is easy to use and calibrate and the parameters A, n, and m must be determined by experiment. To be able to model orthotropic creep, the *POTENTIAL option in ABAQUS was used to specify the stress ratios R_{ij} appearing in Eq. (3.28). The parameters R_{11}, R_{22}, and R_{12}, need to be experimentally determined. However, R_{12} is too difficult to determine by experiment. Therefore, R_{12} was weighted for the modulus of elasticity and the shear modulus, according to $R_{12} = R_{11}G_{12}/E_1$.

The theories of Boltzmann, Schapery, and mechano-sorptive creeping are neglected and have no influence of this model. Due to limitation of the master's dissertation, the creep model of S. Ormarsson [17], was not tested.

6.3. Parameter Study of Creep Model

To determine the parameters of the creep model, chosen for simulating bulging of packages, the parameters were fitted to the experimental data by the aid of the FE-method. Further information of the FE-method can be found in Chapter 7.

In Section 3.5, a detailed description of the material model chosen to describe the creep behavior of the materials in a package is carried out. The creep rate $\dot{\epsilon}^{cr}$, is given once more as

$$\dot{\epsilon}^{cr} = A\tilde{q}^n t^m \tag{6.1}$$

where the constraints

$$A > 0;$$
$$n > 0;$$
$$-1 > m > 0;$$

hold for the parameters.

To determine the influence of the parameters of the creep model on the shape of the resulting creep curve, a parameter study was performed in ABAQUS. A set of parameters were selected as a reference case and then by modifying either A, n, or m, case 1, 2, and 3 was obtained, respectively. For each case, a simulation with the aid of ABAQUS was made. The results from the four cases are shown in Figure 6.1 and Tab. 6.1.

Table 6.1: *The parameters chosen for the four cases in the parameter study.*

	A	n	m
Ref	$4.2089 \cdot 10^{-21}$	2.31	-0.98
case 1	$9 \cdot 10^{-21}$	2.31	-0.98
case 2	$4.2089 \cdot 10^{-21}$	2.2	-0.98
case 3	$4.2089 \cdot 10^{-21}$	2.31	-0.95

From Figure 6.1, it can be concluded that the parameter **A** determines the level of the overall creep-deformations, whereas the parameter **m** changes the curvature. Further, **n** describes how the creep rate depends on the stress level.

6.4. Fitting of Creep Model Parameters to Experimental Data

The fitting process comprises the calibration of the materials of aluminium, polymer, and paper, as well as the whole laminate. The paper and the laminate consider the material directions of MD and CD.

The approach of the fitting procedure was to calibrate the corresponding strips modelled in the FE-program ABAQUS to the experimental data, presented in Chapter 5. By exposing the modelled strip to the same stress-level, exposed to the specimens in the experimental tests, calibration was viable by fitting the parameters of the material model
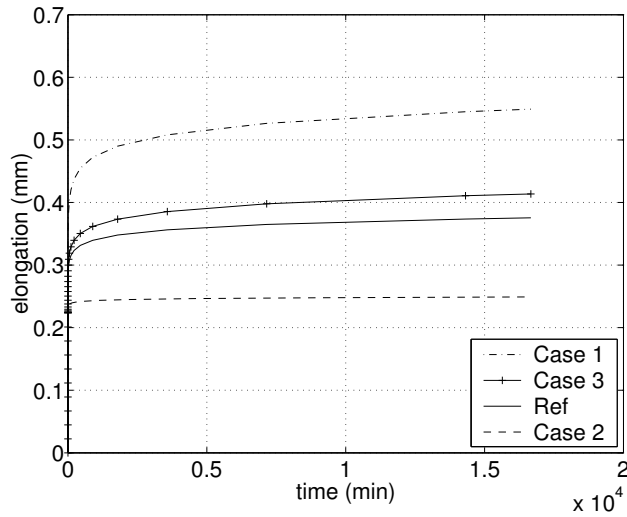
Figure 6.1: *The influence of the parameters A, n, and m, on the creep curve.*

in Eq. (6.1), to the experimental data. In Figure 6.2, the modelled specimen adopts the cross-section, thickness, and fixed length, of the specimens used in the experimental study.
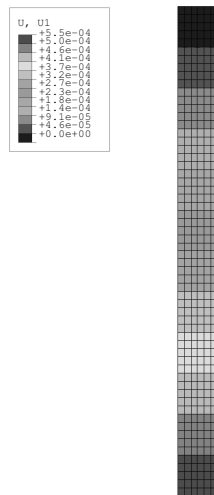
Figure 6.2: *A modelled creep specimen for fitting of experimental data to the creep model.*

6.4.1. Paper

In Figure 6.3-6.5, the fitting of the model parameters to paper is shown as time-elongation curves in at load-levels of 20 N, 40 N, and 50 N, in MD and CD. The load-levels correspond to the stress-levels of 5 MPa, 10 MPa, and 12.5 MPa. It is possible to calibrate an identical curve, with the parameters of the material model, to a single arbitrary creep curve. However, since the same value of the parameters **A**, **n**, and **m** hold for the various load levels, the fitting becomes a compromise between the different load levels and material directions. The overall fitting of the model parameters to paper is better in CD, than in MD. Further, the higher the load-level, the better the fitting. However, the fitting of the model parameters to paper is quite satisfying.

Figure 6.3: *Fitting of the model parameters to paper exerted to a load of 20 N, for MD respectively CD.*

Figure 6.4: *Fitting of the model parameters to paper exerted to a load of 40 N, for MD respectively CD.*

Figure 6.5: *Fitting of the model parameters to paper exerted to a load of 50 N, for MD respectively CD.*

6.4.2. Aluminium

In Figure 6.6, the fitting of the model parameters to aluminium is shown as time-elongation curves. The load-levels of 14 N and 20 N, correspond to 50 MPa, respectively 71 MPa. The fitting becomes a compromise, due to the parameters **A**, **n**, and **m**, hold for either of the load-levels. The fitting of the model parameters to aluminum is overall good, but the fitting of 20 N is somewhat better than the 14 N.
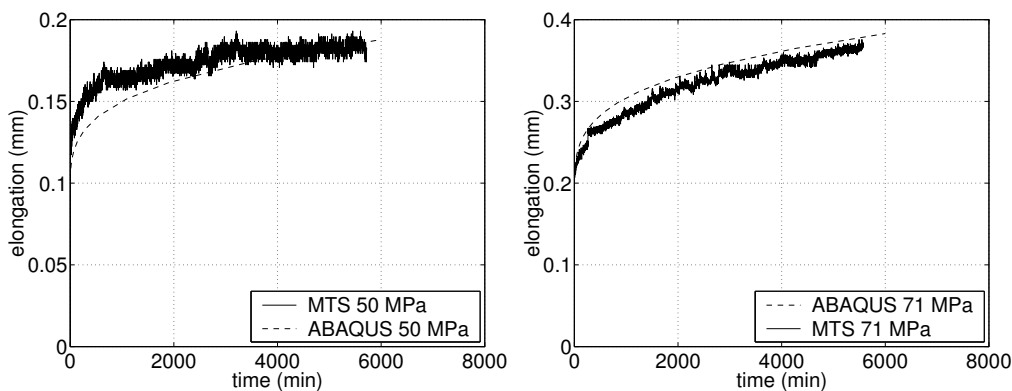
Figure 6.6: *Fitting of aluminium exerted to a load of 14 N respectively 20 N.*

6.4.3. Laminate

The fitting of the model parameters to the laminate, shown in Figure 6.7-6.8, is unsatisfactory. Even though the fitting of the materials in the laminate are satisfying, the fitting to the laminate is not. Possible sources of error, are the material spreading of the laminate

or some errors made in the measurement. Another source of error, is the experimental study of aluminium, where a 14 μm foil was used instead of the original 9 μm foil of the laminate. Thus, a different thickness and quality was used in the creep tests. There is no room for an investigation of the possible sources of error, within this thesis.

The laminate was exposed to the load-levels of 40 N and 50 N, corresponding 10 MPa and 12.5 MPa, respectively. The values of **A**, **n**, and **m**, hold for the various load-levels and material directions. The fitting is considerably better in CD than in MD. There is no big difference in accuracy of the fitting of the two load-levels.
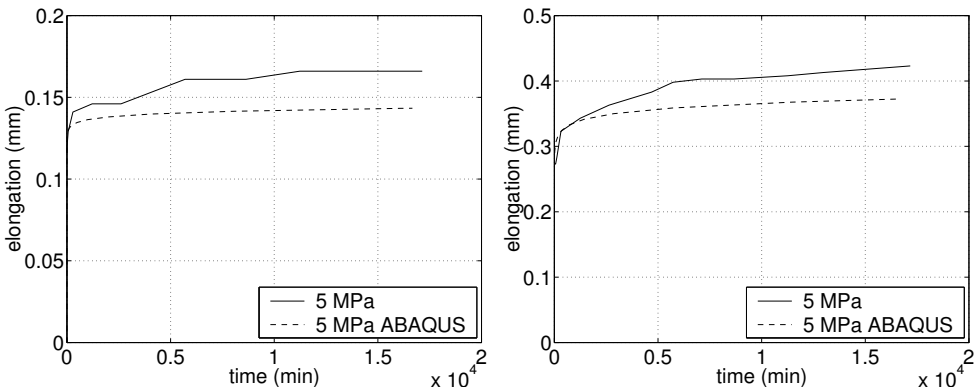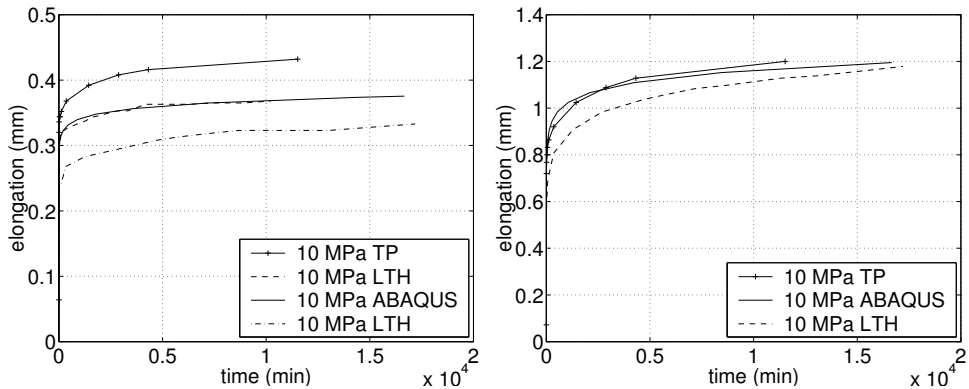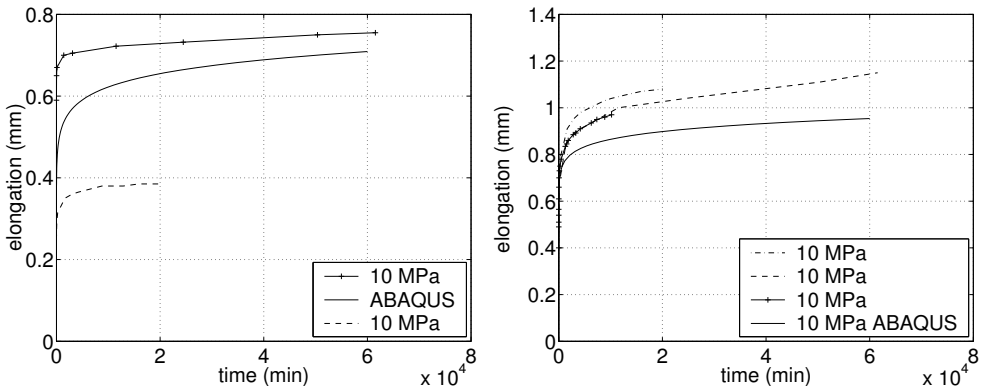

Figure 6.7: *Fitting of the model parameters to laminate exerted to a load of 40 N, for MD respectively CD.*

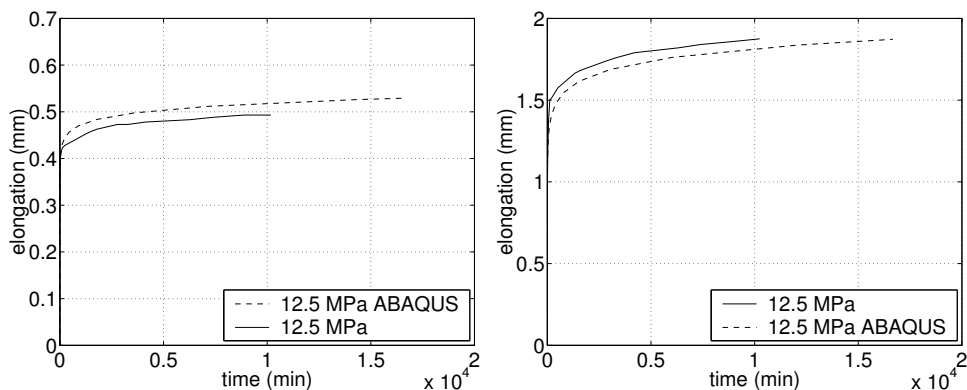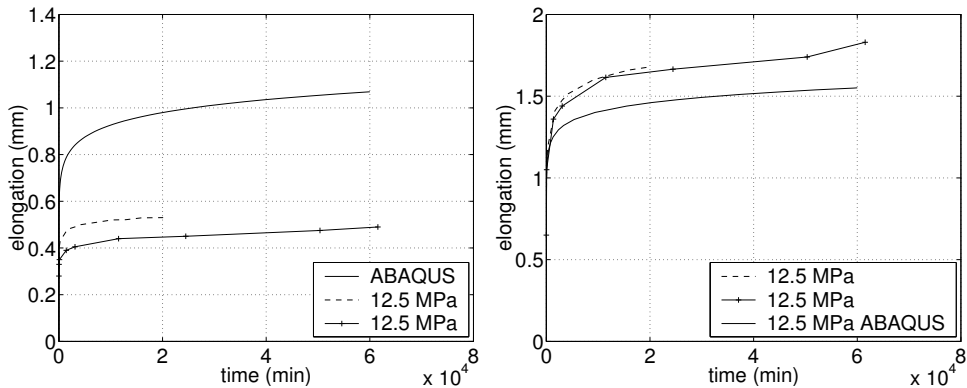Figure 6.8: *Fitting of the model parameters to laminate exerted to a load of 50 N, for MD respectively CD.*

6.4.4. Polymer

In Figure 6.9, the fitting of the model parameters to the polymer HDPE (High Density Polyethylene) is presented. The loads 10 N and 18 N, correspond to the stress-levels of 4.5 MPa and 8 MPa. The values of **A**, **n**, and **m**, hold for the various load-levels. The fitting of the model parameters to the polymer is satisfying. However, the fitting is most suitable to the load-level of 10 N.
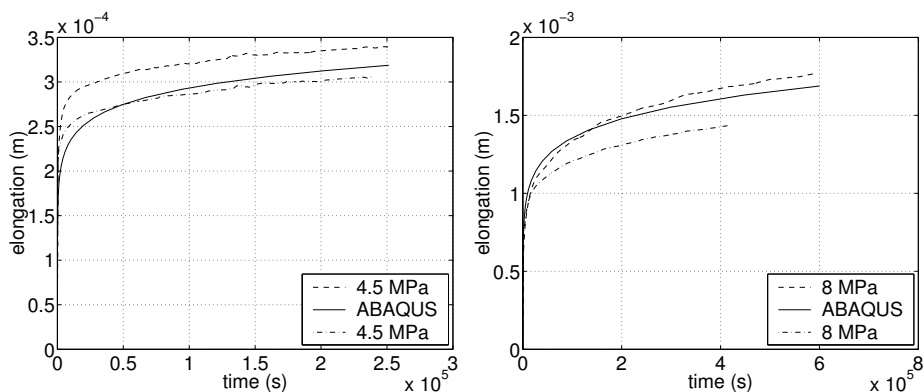
Figure 6.9: *Fitting of the model parameters to polymer exerted to a load of 10 N respectively 18 N.*

6.4.5. Summary

In Tab. 6.2, the parameters A, n, and m are presented for paper, aluminium, and HDPE (High Density Polyethylene). **A** determines the level of the overall creep-deformations, whereas the parameter **m** changes the curvature. Further, **n** describes how the creep rate depends on the stress level.

Table 6.2: *The parameters A, n, and, m presented for each material.*

Parameter	Paper	Aluminium	HDPE
A	$4.2089 \cdot 10^{-21}$	$2.2 \cdot 10^{-21}$	$2.2 \cdot 10^{-20}$
n	2.31	2.0	2.52
m	-0.98	-0.72	-0.96

7. FE-modelling

7.1. General Remarks

It is necessary to simulate the function and strength of the package early in the development process, preferably integrated in the entire product development process, to have a decisive influence on the time of development and future properties. The necessity of prototypes diminish and testing can be focussed on the most important matters. Thus, the product development becomes faster and more cost-effective.

As experimental creep tests require long time frames, it is important to be able to anticipate the creep behavior with a mathematical model. The FE-method is an excellent tool in order to describe, understand, and predict the phenomena of creep.

This chapter contains an exposition of the FE-model describing simulation of bulging. Numerical examples of the simulation, are also presented. The commercial general purpose finite element program, ABAQUS, was used for all calculations.

7.2. FE-method

The Finite Element Method (FEM), is a numerical method by which general differential equations may be solved. Usually, these equations are impossible to solve in an analytical manner and therefore, the numerical approach is an excellent tool. By introducing the approximation of the displacement field, **a**, in Eq. (7.1), the computional effort reduces at the expense of the accuracy of the solution.

$$\boldsymbol{K} \cdot \boldsymbol{a} = \boldsymbol{f} \tag{7.1}$$

where $\mathbf{K}$ is the stiffness matrix, $\mathbf{a}$ is the displacement vector, and $\mathbf{f}$ is the load vector. The main idea of FEM is that a body or structure is subdivided into a number of elements of a finite size. To each of these elements, an approximation of the displacement field is adopted for the elements. The approximation is most often made by adopting polynomial functions, which may be linear, quadratic, or cubic. Once the degree of the polynomials are selected, the stiffness matrix $\boldsymbol{K^e} \cdot \boldsymbol{a^e} = \boldsymbol{f^e}$ of each element can be determined. In order to obtain an approximate solution for the behavior of the entire body, the elements are assembled to the global equations. The overall data, i.e. force, displacement, and boundary conditions, are associated to the nodes.

The first step of a FE-analysis, is to select the appropriate type of elements and mesh.

However, to make this decision, a thorough physical knowledge of the problem considered is of great importance. For any given type of element, it is obvious the smaller the elements, the greater the accuracy [22].

The FE-method is extremely well suited for computer calculations of differential equations. It can be applicable on diverse physical phenomena, such as heat conduction, diffusion, groundwater flow, and analysis of beams and plates [22]. In this master's dissertation, the bulging phenomena of a liquid filled package is simulated.

7.3. The Specific Package

The beverage package that will be studied by use of the finite element method is a 1000 ml bottle intended for UHT-milk (Ultra Heat Treatment), that will be stored in indoor climate for six months, this amount of time is called shelf life. The top of the package is made of plastic material HDPE (High Density Polyethylene) and is equipped with a plastic screw cap. The remainder of the package is made of a laminate constructed from different types of materials, as presented in Figure 2.3 on page 5. As previously mentioned, in order to facilitate the folding of the material, the laminate is creased where the corners will emerge in the package. Since the product is not yet introduced on the market, it is not possible to show the appearance of the package.

7.4. Geometry

An efficient means to reduce the time required for a FE-analysis, is the use of symmetrical planes. The body is divided at the symmetry planes into a minor part, of which the calculation is performed.
Two symmetrical planes exist in the package and thus a quarter of the package was modelled. Hence, the numbers of elements were reduced with a factor of four. A third horizontal plane is not viable, due to neither the vertical geometry or hydrostatic pressure, from the liquid in the package, are symmetric.

The geometry of the package consists of an octagonal bottom plate, flat front, and backside connected with semicircular sides and uppermost is a plastic top. The geometry is modelled with the pre/post processor ABAQUS/CAE. The laminate is creased at the corners between the flat sections and the semicircular sections. A crease deteriorates the stiffness of the paper, since the paper is damaged in the creased zone. Moreover, the paper is bent, and therefore, acts like a compressed spring, with a spring back force, called residual moment.

To incorporate the residual moment into the model, a subroutine implemented by Måns Danelius and Kent Persson (at the Division of Structural Mechanics), was utilized. In Appendix B the subroutine is presented. The input parameters needed for the crease
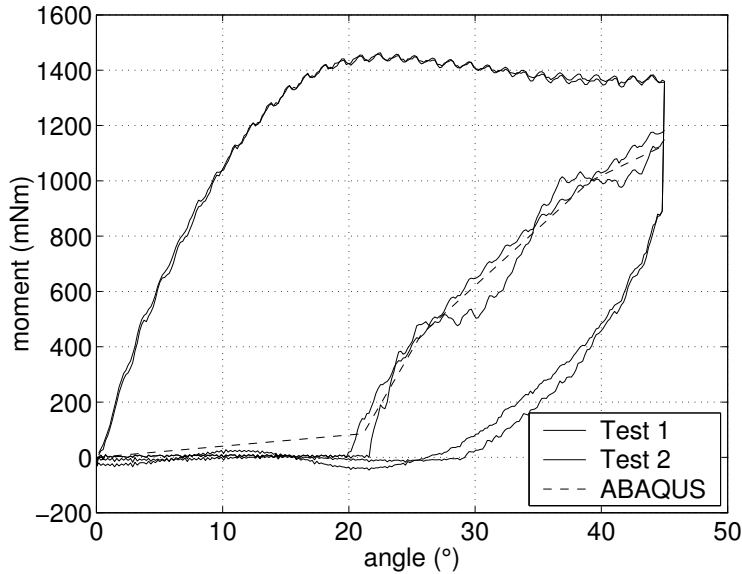
Figure 7.1: *Experimental and model behavior of the moment versus bending angle for a crease.*

model, were the modulus of elasticity in MD and CD, Poisson's ratio in the MD-CD plane, shear modulus in MD-CD-plane, initial curvature of the crease, and finally, a digit indicating the orientation of the crease, 1 for crease in MD and 2 for crease in CD. In Figure 7.1, the moment as a function of the bending angle of the model is shown together with experimental results.

7.5. Element Type and Mesh

The package was modelled with shell elements, where the plastic top was modelled as a homogenous shell and the remainder of the package as a composite shell. A composite shell allows several layers of materials to be defined in an element, where the layers are stacked from the inside to the outside, i.e. in the direction of the normal to the shell.

ABAQUS/CAE comprise various types of mesh techniques as structured, swept, and free. The mesh technique used, was the structured meshing with quadratic element shape, since it allows the best control over the mesh.

In shell elements, plane stress is assumed, which is suitable for thin bodies loaded in the plane. The in-plane stresses σ_{xx}, σ_{yy}, and σ_{xy}, are the only non-zero stresses, whereas the non-zero strains are ϵ_{xx}, ϵ_{yy}, ϵ_{zz}, and γ_{xy}.

The S4R elements were chosen, which is a four-node linear doubly curved thin shell with

reduced integration, hourglass control, and finite membrane strains. Reduced integration means that the numerical integration scheme is of one order less than required for full integration of the selected interpolation. The advantage of the reduced integration is that it gives a more accurate element stiffness, a decrease of the analysis cost, and at the same time, it provides a more accurate stress prediction. However, a serious disadvantage is it can result in a mesh instability, called "hourglassing", which produce zero-energy modes, that cause no straining at the integration points, resulting in an inaccurate solution. To suppress the excessive deformations, hourglass control was employed that affiliates a small artificial stiffness to the the zero-energy deformation modes [15].

7.6. Materials

In order to simulate creep, the power-law model in conjunction with the *POTENTIAL option, describing orthotropy as described in Section 3.5 and Chapter 6, was used.

The parameters A, n, and, m in the model, were chosen according to the experimentally fitted data as described in Chapter 6. In Tab. 7.1, the calibrated parameters A, n, and, m of paper, aluminium, and polymer (HDPE) that were used for the model are presented.

Table 7.1: *The parameters A, n, and, m presented for each material.*

Parameter	Paper	Aluminium	HDPE
A	$4.2089 \cdot 10^{-21}$	$2.2 \cdot 10^{-21}$	$2.2 \cdot 10^{-20}$
n	2.31	2.0	2.52
m	-0.98	-0.72	-0.96
R_{11}	1	-	-
R_{22}	0.55	-	-
R_{12}	0.24	-	-

To obtain a model that produce accurate results, reliable material data is required. The parameters required by the FE-model apart from the creep parameters A, n, m, R_{11}, R_{22}, and R_{12}, are the modulus of elasticity, the shear modulus, and the Poisson's ratio of the materials. Since aluminium and HDPE are considered as isotropic, no values of R_{ij} is needed.

The material data of paper, employed in the FE-model, is presented in Tab. 7.2, where t, E_1, and E_2, were chosen on the basis of the experimental results, presented in the material characterization in Chapter 5. The other parameters were taken from the literature [19].

The material data in Tab. 7.3 was obtained from Tetra Pak. Material data of aluminium, LDPE (Low Density Polyethylene), and HDPE (High Density Polyethylene), were also required by the FE-model. LDPE is used in the laminate and HDPE in the plastic top. As the paper material is orthotropic, the orientation of the material must be considered. Thus, a local material coordinate system is defined for each part, shown in Figure 7.2.

Table 7.2: *Material data chosen for paper.*

Parameter	Paper
t [μm]	395
E_1 [MPa]	5121
E_2 [MPa]	2670
E_3 [MPa]	17
ν_{12}	0.38
ν_{13}	-2.2
ν_{23}	0.54
G_{12} [MPa]	1230
G_{13} [MPa]	8.8
G_{23} [MPa]	8

Table 7.3: *Material data of aluminium, LDPE (Low Density Polyethylene), and HDPE (High Density Polyethylene).*

Parameter	Aluminium	LDPE	HDPE
t [μm]	9	13	305
E [MPa]	70 000	150	894
ν	0.3	0.35	0.38

The material orientation is then aligned with the local coordinate system. This is not the case, for the isotropic materials (aluminium and plastics), where no direction have to be considered.
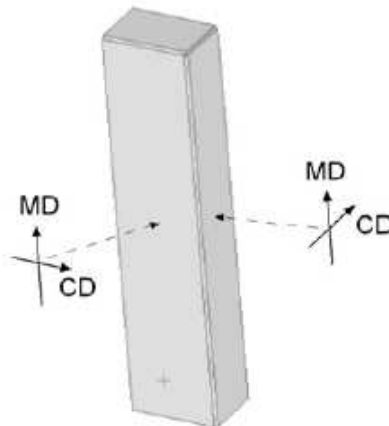
Figure 7.2: *The material orientations of an arbitrary package [1].*

7.7. Loads, Boundary Conditions, and Steps

Since bulging of an open package was simulated, it was sufficient to simulate the loading from the fluid by applying an interior hydrostatic pressure only. Hydrostatic pressure p, may be written as

$$p = \rho g h \tag{7.2}$$

where ρ is the density of the liquid, g acceleration of gravity, and h is the hydrostatic pressure height.

At the symmetry boundaries, boundary conditions were applied, according to Figure 7.3. The bottom was constrained in the vertical direction. Initially, boundary conditions were imposed around the crease.

Since large deformations occured, a geometric non-linear analysis was performed. The geometric non-linear analysis is based on equilibrium on deformed geometry. This type of analysis is requested by including the *NLGEOM option in ABAQUS, to the model. A non-linear geometric FE-analysis requires a great computional effort and is for that reason rather time demanding.
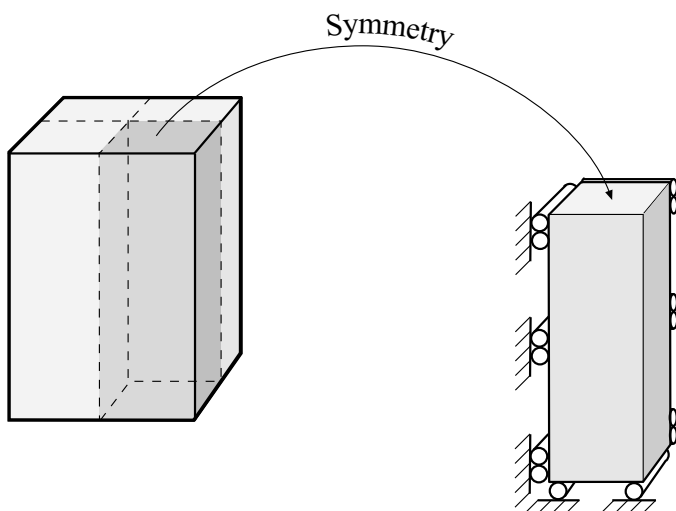

Figure 7.3: *The boundary conditions introduced to the model.*

To analyze the model, several analysis steps were needed to be defined. The step sequence provided a convenient way to capture changes in the loading and boundary conditions of the model, during the course of the analysis.

The simulation of bulging of a beverage package, was divided into four analysis steps.

In the first step, the boundary conditions around the crease and the boundary conditions shown in Figure 7.3, were imposed on the model. Further, the residual moments were applied to the crease by the aid of a subroutine, which is presented in Appendix A. The next analysis step involved the removal of the boundary conditions of the crease. Thus, the residual moments were exerted to the whole package, causing the package to change its shape. In the third step, the only load exerted to the package, was the hydrostatic pressure, where the hydrostatic height was the origin of the load. Eventually, in step four, the package was allowed to creep. This step was however, rather time demanding.

The simulation of bulging was made in the following four analysis-steps:

- Step 1: Introduction of boundary conditions and residual moments from the creases.

- Step 2: Removal of the BC around the creases.

- Step 3: The hydrostatic pressure was introduced.

- Step 4: Viscoelastic step, the creep simulation of the package.

where the first three steps are static.

7.8. Numerical Examples

It is of great interest to compare the FE-model, presented in Chapter 7, to the bulge tests performed in Section 5.8. Therefore, three numerical examples were carried out. The two first examples display the instantaneous bulging after eight days and nine weeks, respectively. In the third example, the creep deformation over time, for a certain point is presented.

In Figure 7.4 and 7.5, a comparison of simulations with bulge test results are shown for empty and filled packages. The bulge test curves are actually mean value curves of five bulge tests. After eight days, the ABAQUS simulations show a satisfying agreement with the bulge tests, as can be seen in Figure 7.4. In Figure 7.5, after nine weeks of creep, the agreement between simulations and experimental data is acceptable. With a discrepancy of 1/10 mm in width after nine weeks, the simulation gives an acceptable description of the creep behavior.

In order to display bulging with a time scale, the creep deformation at a certain point of the package is considered. This point is located at an altitude of 100 mm, on the symmetrical section on the flat side of the package. The packages were allowed to creep for nine weeks. Figure 7.6 presents the creep deformation over time for the simulation and the bulge tests. When comparing the results in Figure 7.6 with the results in Figure 7.5, the creep deformation of the ABAQUS simulation, seems to be somewhat too large.
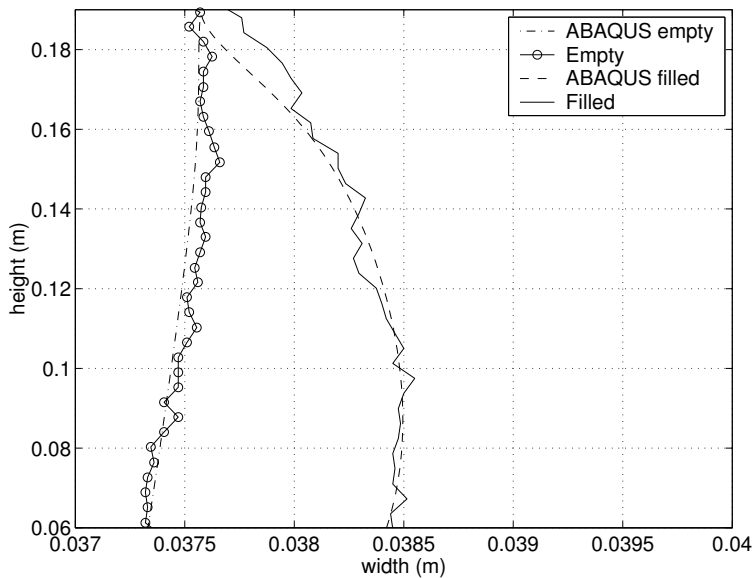
Figure 7.4: *Bulging after eight days.*
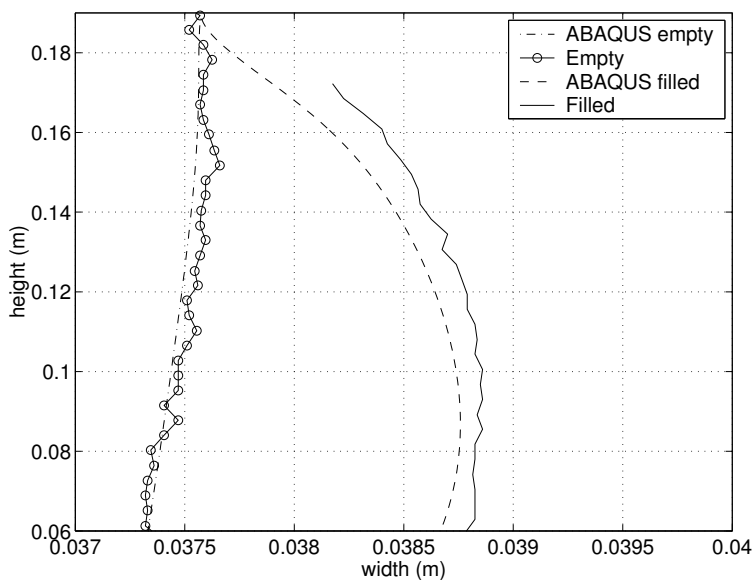
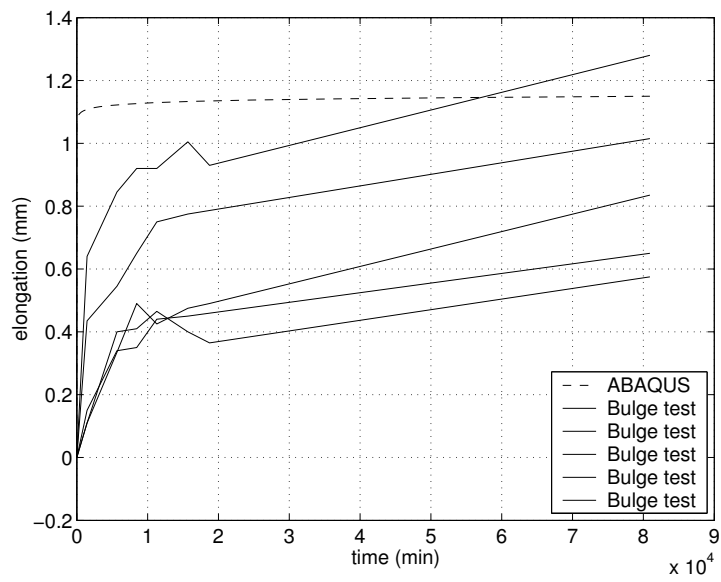Figure 7.5: *Bulging after nine weeks.*

Figure 7.6: *Creep deformation over time, for a certain point.*

8. Results and Discussion

In this master's thesis, a FE-model for simulation of creep in beverage packages has been developed. The FE-model was proven to produce accurate results for shorter time periods and acceptable results for longer time frames, but still, further work and resources are required to achieve a model that will provide accurate results for longer time frames.
The benefit of a carefully calibrated FE-model, is the prediction of the creep behavior. Thus, the product development becomes faster and more cost-effective.

Within the FE-model, the material model chosen was the Power-law model and the compiled parameters governing the creep curve are presented in Tab. 8.1, for paper, aluminium, and HDPE (High Density Polyethylene).

Table 8.1: *The parameters A, n, and, m presented for each material.*

Parameter	Paper	Aluminium	HDPE
A	$4.2089{\cdot}10^{-21}$	$2.2{\cdot}10^{-21}$	$2.2{\cdot}10^{-20}$
n	2.31	2.0	2.52
m	-0.98	-0.72	-0.96

The conclusion of the experimental study in Chapter 5, was that the creep deformation is approximately four to six times larger in CD, than in MD. Thus, the bulging depends on how the paper is oriented in the package.

The numerical examples of bulging presented in Section 7.8, showed a slightly disagreement as compared to the experimental results of the bulge tests. The major cause of the disagreement is probably that the creep of the laminate was underestimated in the simulation. This may due to several factors.
The FE-model was calibrated to the experimental data of the materials in the laminate. In the experimental study, the materials of the laminate were allowed to creep for approximately two weeks. Preferably, the FE-model should have been calibrated to experimental data of three months, in order to consider the logarithmic behavior of creep.
The experimental study of aluminium, was performed on a 14 μm foil of somewhat different quality than the original 9 μm aluminium foil in the laminate. Thus, a different quality and thickness was used in the creep tests. Therefore, the result of the creep behavior of the aluminium foil may differ from the behavior of the actual aluminium foil in the laminate.
The moisture content of the paper in the laminate, may have been changing during the elapsed time of the bulge tests. Therefore, the significance of a moisture-dependent FE-

model, which also includes mechano-sorptive creeping, is decisive to be able to perform an accurate simulation of bulging.

8.1. Proposals for Future Work

Proposals for future work and for the continuation of the work made in this thesis are,

- The creep model presented in literature [17], is originally established for the creep of timber, but may also be suitable to describe creep of paper. A suggestion is to calibrate this model and to see if it is possible to describe creep of paper.

- A numerical and experimental parameter study of the laminate, to obtain a more accurate calibration of the model parameters to the laminate.

- Simulation of bulging on sealed and stacked packages with fluid elements, which is more close to a real loading scenario for bulging.

- Development of moisture-dependent models. The significance of a moisture-dependent FE-model, which also includes mechano-sorptive creeping, is decisive to be able to perform an accurate simulation of bulging.

Bibliography

[1] Eskil Andreasson and Ted Bengtsson. *Grip stiffness of beverage packages - An Experimental and Finite Element Study.* Div. of Structural Mechanics, Lund University, Lund 2002.

[2] Svensk Standard SS152005 Utgåva 4, TNC 92. *Pappersordlista/Paper Vocabulary.* SIS Tryckeri, Stockholm 1992.

[3] Johan Renström. *FEM-modellering av bantransport för trycktekniska tillämpningar.* KTH Solid Mechanics, Stockholm 1998.

[4] Kevin P. Menard. *Dynamical mechanical analysis.* CRC Press LLC, Boca Raton 1999.

[5] Gert Hedner. *Formelsamling i hållfasthetslära.* Civiltryck AB, Stockholm 1986.

[6] Damir Krusvar. *Olinjär krypning hos papper - modellering och provning.* Div. of Structural Mechanics, Lund University, Lund 1999.

[7] Matti Ristinmaa. *The mechanics of constitutive modelling.* Div. of Solid Mechanics, Lund University, Lund 1999.

[8] P. Kolseth. *The measurements of viscoelastic behavior for the characterization of time,- temperature and humidity-dependent properties.*

[9] J.M.G Cowie. *Chemistry & Physics of modern materials.*

[10] Edmond P. Saliklis. *Constitutive modeling of paper accounting for rate of load and transient relative humidity effects.* Tappi Journal, NO. 2, 1998.

[11] Richard E. Mark. *Handbook of physical and mechanical testing of paper and paperboard.* Marcel Dekker, inc., New York 1983.

[12] James L. Rand. *A nonlinear viscoelastic creep model.* Tappi Journal, July 1995.

[13] Poorvi Patel. *Nonlinear creep model of paper and corrugated board materials.* Div. of Structural Mechanics, Lund University, Lund 1999.

[14] Jan Lif. *Analysis of the time and humidity-dependent mechanical behavior of paper webs at offset printing press conditions.* KTH Solid mechanics, Stockholm 2003.

[15] ABAQUS Online Documentation *ABAQUS Analysis User's Manual* ABAQUS Inc, 2003.

[16] Kent Persson *Micromechanical modelling of wood and fibre properties* Div. of Structural Mechanics, Lund University, Lund 2000.

[17] Sigurdur Ormarsson. *Numerical analysis of moisture-related distortions in sawn timber.* Div. of Structural Mechanics, Lund University, Lund 1999.

[18] Vincent T. Morgan. *Compressive creep of stacked sheets of paper* Tappi Journal, NO.7, 1994.

[19] Kent Persson. *Material model for paper experimental and theoretical aspects.* Div. of Solid mechanics, Lund University, Lund 1991.

[20] Henry W. Haslach Jr. *The mechanics of moisture accelerated tensile creep in paper.* Tappi Journal, NO.10, 1994.

[21] *Nationalencyklopedin* NE Nationalencyklopedin AB

[22] N. Ottosen and H. Petersson *Introduction to the Finite Element Method.* Prentice Hall, 1992.

A. Subroutine

Subroutines used in ABAQUS need to be implemented in the programming language Fortran. This subroutine was used for describing the moment bending angle relationship of the crease.

```
      SUBROUTINE UGENS (DDNDDE,FORCE,STATEV,SSE,SPD,PNEWDT,STRAN,
     1 DSTRAN,TSS,TIME,DTIME,TEMP,DTEMP,PREDEF,DPRED,CENAME,NDI,
     2 NSHR,NSECV,NSTATV,PROPS,JPROPS,NPROPS,NJPROP, COORDS,CELENT,
     3 THICK,DFGRD,CURV,BASIS,NOEL,NPT,KSTEP,KINC,NIT,LINPER)
C-----------------------------------------------------------------
C   User subroutine "UGENS" to ABAQUS for simulating the non-linear
C   moment-curvature relation and residual moment of creases.
C-----------------------------------------------------------------
C   Props(1) = Emd  , Modulus of elasticity in MD
C   Props(2) = Ecd  , Modulus of elasticity in CD
C   Props(3) = vmdcd, Poissons ratio md-cd
C   Props(4) = Gmdcd, Shear modulus in md-cd-plane
C   Props(5) = Initial curvature of crease
C   Jprops(1) = 1 or 2. 1 for crease in MD. 2 for crease in CD.
C-----------------------------------------------------------------
C
      IMPLICIT REAL*8(A-H,O-Z)
      CHARACTER*80 CENAME
      DIMENSION DDNDDE(NSECV,NSECV),FORCE(NSECV),STATEV(NSTATV),
     1 STRAN(NSECV),DSTRAN(NSECV),TSS(2),TIME(2),PREDEF(*),
     2 DPRED(*),PROPS(4),JPROPS(*),COORDS(3),DFGRD(3,3),
     3 CURV(2,2),BASIS(3,3)
C
      REAL*8 DFORCE(1:6), DSTRAN1(1:6)
      PARAMETER(NPRECD=2)
      LOGICAL OP
C
C   Definitions for crease in MD
C
      IF (JPROPS(1).EQ.1) THEN
C
C   Definition of stiffness matrix
C
      DO 10 I=1,6
        DO 20 J=1,6
          DDNDDE(I,J)=0D0
  20    CONTINUE
  10  CONTINUE

C
      C11=1/PROPS(1)
      C22=1/PROPS(2)
      C21=PROPS(3)/PROPS(1)
      A=1/(C11*C22-C21**2)
      B=(THICK**3)/12
      DDNDDE(1,1)=THICK*C22*A
      DDNDDE(1,2)=THICK*C21*A
```

```
      DDNDDE(2,1)=THICK*C21*A
      DDNDDE(2,2)=THICK*C11*A
      DDNDDE(3,3)=THICK*PROPS(4)
      DDNDDE(4,4)=B*C22*A
      DDNDDE(5,5)=B*C11*A
      DDNDDE(6,6)=B*PROPS(4)
C
      D1=8.1E-6
    D2=156.3E-6
    D3=83.0E-6
    D4=45.0E-6
C
      B1=85.7E-3
    B2=442.9E-3
    B3=1000E-3
C
C    Setting curvature in first increment for determination
C    of residual moment
C
      IF (KINC.EQ.1 .AND. KSTEP.EQ.1) THEN
          STRAN(5)=PROPS(5)
      ENDIF
C
C    Calculation of incremental forces and moments
C
      CALL MULT(DDNDDE,DSTRAN,DFORCE)
      DO 30 K=1,6
            FORCE(K)=FORCE(K)+DFORCE(K)
 30    CONTINUE
C
C    Calculation of stiffness and moment for crease
C
      TSTRAN=(STRAN(5)+DSTRAN(5))
C
      IF (TSTRAN.LT. B1) THEN
         DDNDDE(5,5)=D1
         FORCE(5)=D1*TSTRAN
      ELSEIF (TSTRAN .GE. B1 .AND. TSTRAN .LT. B2) THEN
         DDNDDE(5,5)=D2
         FORCE(5)=D1*B1+D2*(TSTRAN-B1)
      ELSEIF (TSTRAN .GE. B2 .AND. TSTRAN .LT. B3) THEN
        DDNDDE(5,5)=D3
         FORCE(5)=D1*B1+D2*(B2-B1)+D3*(TSTRAN-B2)
    ELSEIF (TSTRAN.GE. B3) THEN
        DDNDDE(5,5)=D4
         FORCE(5)=D1*B1+D2*(B2-B1)+D3*(B3-B2)+D4*(TSTRAN-B3)
      ENDIF
```

```
C    end crease in MD
C
C    Definitions for crease in CD
C
      ELSEIF(JPROPS(1).EQ.2)THEN
C
C    Definition of stiffness matrix
C
      DO 40 I=1,6
        DO 50 J=1,6
          DDNDDE(I,J)=0D0
  50    CONTINUE
  40  CONTINUE


C
      C11=1/PROPS(1)
      C22=1/PROPS(2)
      C21=PROPS(3)/PROPS(1)
      A=1/(C11*C22-C21**2)
      B=(THICK**3)/12
      DDNDDE(1,1)=THICK*C22*A
      DDNDDE(1,2)=THICK*C21*A
      DDNDDE(2,1)=THICK*C21*A
      DDNDDE(2,2)=THICK*C11*A
      DDNDDE(3,3)=THICK*PROPS(4)
      DDNDDE(4,4)=B*C22*A
      DDNDDE(5,5)=B*C11*A
      DDNDDE(6,6)=B*PROPS(4)
C
      D1=8.1E-6
    D2=156.3E-6
    D3=83.0E-6
    D4=45.0E-6
C
      B1=85.7E-3
    B2=442.9E-3
    B3=1000E-3
C
C    Setting curvature in first increment for determination
C    of residual moment
C
      IF (KINC.EQ.1 .AND. KSTEP.EQ.1) THEN
          STRAN(4)=PROPS(5)
      ENDIF
C
C    Calculation of incremental forces and moments
C
```

```fortran
      CALL MULT(DDNDDE,DSTRAN,DFORCE)
      DO 60 K=1,6
            FORCE(K)=FORCE(K)+DFORCE(K)
 60   CONTINUE
C
C    Calculation of stiffness and moment for crease
C
      TSTRAN=(STRAN(4)+DSTRAN(4))
C
      IF (TSTRAN.LT. B1) THEN
         DDNDDE(4,4)=D1
         FORCE(4)=D1*TSTRAN
      ELSEIF (TSTRAN .GE. B1 .AND. TSTRAN .LT. B2) THEN
         DDNDDE(4,4)=D2
         FORCE(4)=D1*B1+D2*(TSTRAN-B1)
      ELSEIF (TSTRAN .GE. B2 .AND. TSTRAN .LT. B3) THEN
        DDNDDE(4,4)=D3
         FORCE(4)=D1*B1+D2*(B2-B1)+D3*(TSTRAN-B2)
    ELSEIF (TSTRAN.GE. B3) THEN
        DDNDDE(4,4)=D4
         FORCE(4)=D1*B1+D2*(B2-B1)+D3*(B3-B2)+D4*(TSTRAN-B3)
      ENDIF
C   end crease in CD
C
    ENDIF
      RETURN
    END
C.....................................................
C   SUBRUTIN MATRIX MULTIPLICATION, A*B=C
C
      SUBROUTINE MULT(A,B,C)
C
      IMPLICIT REAL*8(A-H,O-Z)
      DIMENSION A(6,6),B(6),C(6)
C
      DO 4 I=1,6
         E=0
       DO 3 J=1,6
 3          E=E+A(I,J)*B(J)
 4      C(I)=E
 5    CONTINUE
      RETURN
      END
```